Title:

SNARE Protein Ykt6 Drives AMPAR Insertion at Synaptic Terminals During LTP

Authors

Momoko Takahashi[1] and Gabriela Caraveo[1]

[1]Department of Neurology, Feinberg School of Medicine, Northwestern University, Chicago, IL, USA

Abstract

Ykt6 is a SNARE protein essential for vesicular fusion along the secretory pathway. It has been implicated in α-synuclein (αSyn) pathology and is critically involved in α-synuclein-dependent dementias. αSyn disrupts AMPA receptor (AMPAR) expression at synaptic terminals, which is key for long-term potentiation (LTP)—the cellular basis of memory and learning. AMPAR expression at synaptic terminals relies on the secretory pathway; however, the role of Ykt6 in LTP and its perturbation under αSyn pathological conditions remain unexplored. Here, we demonstrate that Ykt6 is highly expressed in the hippocampus of the mammalian brain, relocalizes to synaptic terminals during LTP, and regulates GluA1 surface expression. Moreover, we found that Ykt6 modulates the synaptic vesicular pools and dendritic arborization. Taken together, our findings establish Ykt6 as an essential SNARE for hippocampal neural function during LTP, with significant implications for α-synuclein-dependent dementias.

Introduction

Aberrant expression and aggregation of α-synuclein (αSyn) are hallmark features of synucleinopathies which include Dementia with Lewy Bodies (DLB) and Parkinson's Disease Dementia (PDD) (1–6). Deficits in memory are a common feature of these neurodegenerative diseases, yet the underlying cause of dysfunction is largely unexplored.

While the exact role of αSyn has not yet been fully elucidated, pathological levels of αSyn cause hyperactivity of Ca^{2+} and calmodulin dependent serine/threonine phosphatase calcineurin (CaN). Our laboratory and others have found that sustained CaN activity is a critical contributor to cytotoxicity (7–14); however, reducing CaN can rescue the neurotoxic effects of αSyn (15–17). Through an unbiased phosphoproteomic approach, our laboratory previously identified Ykt6 as a substrate of CaN (18). Ykt6, an essential soluble N-ethylmaleimide-sensitive factor attachment protein receptor (SNARE) that has been critically implicated in the pathobiology of αSyn (8, 19, 20), regulates vesicular fusion along the secretory pathway, including transport between the ER and Golgi apparatus, within the Golgi, from the Golgi to the plasma membrane (21, 22), and in autophagy-related vesicular fusion pathways (8, 18, 20, 23–27).

Unlike most SNARE proteins, Ykt6 lacks a transmembrane domain and relies on reversible lipidation for recruitment to membranes to facilitate vesicular fusion. We and others have established that in the inactive state, Ykt6 is localized in the cytosol in a close conformation, whereby the regulatory longin domain is closely associated with the SNARE domain (22, 27–29). In the active state, phosphorylation at the SNARE domain causes an intra-conformational change which separates the longin and the SNARE domain allowing C-terminus lipid modifications (18, 28, 30–34). Reversible lipidation allows Ykt6 to be anchored to the endoplasmic reticulum (ER), Golgi and plasma membranes (30, 31, 33, 35, 36). Our laboratory also discovered that the subsequent dephosphorylation of the SNARE domain by CaN enhances SNARE-SNARE interactions, thereby facilitating vesicular fusion in both the secretory and autophagic pathways (26, 27, 29, 36–38). We also discovered that Ykt6 undergoes constitutive dephosphorylation by CaN under pathological αSyn conditions (9, 18, 34). This disrupts its regulated open and closed conformational cycles, ultimately losing its function. While Ykt6 is selectively expressed in neurons in rat cerebral cortex and the hippocampus (39), whether Ykt6 regulates secretory transport in neurons under physiological and αSyn pathological conditions has been largely unexplored.

The secretory transport not only facilitates dendritic arborization (40–43), but also transports receptors that support synaptic functions (44–52). On synapses, α-amino-3-hydroxy-5-methyl-4-isoxazolepropionic acid (AMPA) receptors (AMPARs) modulate synaptic strength to facilitate

information processing and storage (53–56). AMPARs are rapidly inserted into synapses during long-term potentiation (LTP), a form of synaptic strengthening (57). For this rapid insertion, AMPARs are transported to synaptic vicinities via the secretory pathway (58). While the roles of exocytosis and endocytosis in activity-dependent AMPAR transport at postsynaptic terminals are well-established (48–52), the activity-dependent contribution of the secretory pathway remains poorly understood. Therefore, we asked whether Ykt6, the master regulator of the secretory pathway, participates in delivering AMPARs during LTP. Here we show that Ykt6 is highly expressed in the hippocampus in the mammalian brain. Using primary pyramidal hippocampal neurons, we demonstrate that Ykt6 relocates to synaptic terminals in response to LTP and increases surface levels of GluA1, a subunit of AMPARs. Moreover, we show that Ykt6 regulates the synaptic vesicular pools and acts as a positive regulator of dendritic arborization. Taken together, our findings highlight a critical role for Ykt6 in LTP. Given Ykt6's involvement in αSyn pathobiology, our findings may have therapeutic implications for αSyn-dependent dementias characterized by deficits in memory formation.

Methods

Primary Hippocampal Cultures

Embryonic rat hippocampal neurons were isolated from euthanized pregnant Sprague–Dawley rats at embryonic day 18 using a modified protocol from Lesuisse and Martin. Protocol was approved by Northwestern University administrative panel on laboratory animal care. Embryos were harvested by Caesarean section and hippocampi were isolated and dissociated with 0.25% Trypsin without EDTA (Invitrogen, 15090-046) digestion for 15 min at 37°C and trituration with 1 ml plastic tip. Poly-D-Lysine (Sigma, P-1149)-coated 1.5 coverslips (Neuvitro, GG-12--1.5-oz) in 24-well plates were seeded with 5 x 10^5 cells accordingly in neurobasal medium (Gibco, 21103-049) supplemented with 10% heat-inactivated FBS (Gibco), 0.5 mM glutamine (Gibco), penicillin (100 IU/mL), and streptomycin (100 µg/mL) (Gibco). Before seeding, cells were counted using the automated cell counter TC10 (Bio-Rad) and viability (90-95%) was checked with Trypan Blue Stain (0.4%, Gibco 15250-061). After 1 hour (h) incubation at 37°C, media was changed to neurobasal medium (Gibco, 21103-049) supplemented with B27 (Gibco, 17504-044) and 0.5 mM glutamine. One half (out of 500 µl volume for 24-well plates) of the media was changed on DIVs 5, 9, 12, 16, and 19.

Plasmids

Nontargeting ShRNA (Horizon Discovery Dharmacon, VSC11656) or ShRNA targeting Ykt6 (Horizon Discovery Dharmacon, V3SH7669) were expressed in mammalian cells using lentiviral induction at DIV 5.

Expression was verified visually by the expression of turboRFP.

Human eGFP-Ykt6 (a kind gift from Dr. Joseph Mazzulli, Northwestern University) and eGFP were expressed in mammalian cells using lentiviral induction at DIV 5 at half the MOI used with ShRNAs.

Doxycycline treatment of cultures

Primary hippocampal cultures that were infected with either nontargeting ShRNA or ShRNA targeting Ykt6 were treated with doxycycline. Targeted silencing of Ykt6 in primary hippocampal cultures was induced using doxycycline treatments at a concentration of 1nM at DIV7, 11, 14, 18 and 21 before used for experiments. Viral MOI and doxycycline titrations were performed on new batches before applied experimentally and confirmation of knockdown and expression of turbo RFP was regulated.

Chemical LTP induction

The samples were washed once with warmed extracellular solution (ECS) containing (in mM): 150 NaCl, 2 $CaCl_2$, 5 KCl, 10 HEPES, 30 Glucose, 0.001 TTX, 0.01 strychnine, and 0.03 picrotoxin at pH 7.4, then exposed to 300μM glycine in ECS for 3 minutes (external/internal staining) or 6 minutes (western blot) at room temperature, then washed with extracellular solution thrice, then incubated at 37°C for 20 minutes prior to further processing.

External/Internal Staining

External and internal glutamatergic receptors were stained according to the protocol by Chiu. et.al (59). Coverslips with primary hippocampal cultures were transferred to parafilm-covered dishes and incubated in primary antibody (GluA1: Invitrogen, MA5-27694; GluN1: Alomone Labs, AGC-001) at the concentration of 1:100 diluted in conditioned media for 15 minutes at room temperature, then washed three times with warm conditioned media. The coverslips were then washed once with phospho-buffered saline (PBS) supplemented with 1mM $MgCl_2$ and 0.1mM $CaCl_2$ (PBS+). The cells were then fixed by incubating with fresh 4% paraformaldehyde (PFA) and 4% sucrose in PBS for 8 minutes. The cells were then washed three times with PBS, then blocked with 10% normal goat serum (NGS) in PBS for minimum 30 minutes at room temperature. The cells were then incubated with 1:400 dilution of goat anti-mouse Alexa Fluor® 405 secondary antibody (Invitrogen, A-31553) or goat anti-rabbit Alexa Fluor® 405 secondary antibody (abcam, ab175652) in 3% NGS in PBS for 1 hour at room temperature. The cells were then washed 3 times with PBS.

For internal staining, the cells were then permeabilized with 0.25% Triton X-100 (Thermo Fisher Chemicals, A16046.AP) for 7 minutes at room temperature, then blocked with 10% NGS in PBS for minimum 30 minutes at room temperature. The intracellular receptors were then labelled by incubating the cells with the same primary antibodies at the same concentration, and anti-microtubule-associated protein 2 (MAP2) chicken antibody (abcam, ab318993) at 1:10000 dilution,

but diluted in 3% NGS in PBS overnight in 4°C. The next morning, cells were washed 3 times with PBS, then labelled with goat anti-mouse Alexa Fluor® 647 secondary antibody (Invitrogen, A-21235) or goat anti-rabbit Alexa Fluor® 405 secondary antibody (Invitrogen, A-21245) at 1:1000 dilution and goat anti-chicken Alexa Fluor® 488 secondary antibody (Invitrogen, A-11039) at 1:400 dilution in 3% NGS in PBS for 1 hour at room temperature. The cells were then washed 3 times with PBS and once with de-ionized water, then mounted using Prolong Gold antifade mountant (Invitrogen, P36930). The cells were imaged using Nikon A1R GaAsP point-scanning laser confocal microscope using 63x oil-immersion objective (NA = 1.4) with z-series of 10-20 images, taken at 0.3 µm intervals, with 2048x2048 pixel resolution. Only cells positive for MAP2 were acquired. The external to internal expression ratio was calculated for the basal condition with GFP and Sh Ctrl, or Sh Ctrl only. This value was then normalized to 1, and all other ratios normalized to the basal condition.

Ykt6 Staining

Primary hippocampal cultures as described above at DIV21 were washed once with PBS+, then fixed with fresh 4% PFA and 4% in sucrose in PBS for 20 minutes at room temperature. They were then permeabilized with 0.3% Triton-X 100 in PBS for 30 minutes at room temperature. The cells were blocked with 0.3% Triton-X 100/2% bovine serum albumin (BSA)/5% NGS in PBS for 30 minutes, then incubated for 48 hours at with mouse v-SNARE Ykt6p antibody (Santa Cruz, sc-365732), rabbit anti-Ykt6 primary antibody (abcam, ab236583), purified mouse anti-GM130 primary antibody (BD Biosciences, 610822) at 1:200 dilution, or rabbit anti-PDI primary antibody (Cell Signaling Technology, 3501), all at 1:100 dilution in the blocking buffer. Anti-microtubule-associated protein 2 (MAP2) chicken antibody (abcam, ab318993) at 1:10000 dilution was used to identify neurons. For PSD95, mouse anti-PSD95 primary antibody (Invitrogen, MA1-045) was used at 1:400 dilution.

After primary incubation, cells were washed three times with 0.05% Tween-20 in PBS for 15 minutes each, then with PBS twice for 15 minutes each, then incubated with then labelled with goat anti-mouse Alexa Fluor® 647 secondary antibody (Invitrogen, A-21235) or goat anti-rabbit Alexa Fluor® 405 secondary antibody (Invitrogen, A-21245) at 1:5000 dilution and goat anti-chicken Alexa Fluor® 488 secondary antibody (Invitrogen, A-11039) at 1:400 dilution in the blocking buffer for 2 hour at 4°C. The coverslips were then washed three times with 0.05% Tween-20 in PBS for 15 minutes each, and then twice in PBS for 15 minutes each, and mounted with Prolong Gold Antifade mountant. The cells were imaged using Nikon A1R GaAsP point-scanning laser confocal microscope using 63x oil-immersion objective (NA = 1.4) with z-series of 10-20 images, taken at 0.3 µm intervals, with 2048x2048 pixel resolution. Only cells positive for MAP2 were acquired.

Sholl Analysis

Scholl Analysis was performed in cultured rat primary hippocampal cultures. Neurons were plated and allowed to mature until DIV21 and transfected with PGK-mCherry using Lipofectamine 2000 according to manufacturer's protocol at DIV 16. At DIV21 they were washed once with PBS+, fixed with fresh 4% PFA and 4% in sucrose in PBS. They were then permeabilized with 0.3% Triton-X 100 in PBS for 7 minutes at room temperature, blocked with 3% NGS in PBS, and then stained with anti-mCherry primary antibody (Abcam ab167453) at the concentration of 1:400 diluted in 3% NGS in PBS. overnight in 4°C.

The next day, the coverslips were incubated with Goat Anti-Rabbit Alexa Fluor® 594 secondary antibody (abcam, ab150080) at 1:500 concentration diluted in 3% NGS in PBS, washed 3 times with PBS, and then mounted using Prolong Gold Antifade mountant. Isolated neurons were imaged using Nikon A1R GaAsP point-scanning laser confocal microscope using 63x oil-immersion objective (NA = 1.4) with z-series of 8–10 images, taken at 0.3 μm intervals, with 1024 × 1024 pixel resolution. The stacks were then flattened to 1 image in ImageJ and Scholl Analysis performed using the SNT plugin (ImageJ)(60) after manual tracing.

Ykt6/Organelle Analysis

To measure the relative intensities of Ykt6 and the respective organelles, ImageJ was used with the ColorProfiler plugin. For the soma, a line was drawn in between the beginnings of the basal dendrites of the hippocampal neurons. For the dendrites, the line was drawn across the width of the secondary dendrite, immediately after the bifurcation point.

PSD95 distance measurement

To measure the distance between post-synaptic density 95 (PSD95) puncta and its most proximate Ykt6 puncta, coverslips were incubated per protocol above using the mouse anti-PSD95 and the rabbit anti-Ykt6 antibodies at given concentrations. The coverslips were imaged on Nikon AXR point-scanning laser confocal microscope using 100x (NA=1.49), with 2048x2048 pixel resolution. The images were analysed using ImageJ (61) and Colocalization by Cross Correlation package by McCall (62), by first constructing a mask to extrapolate the secondary dendrite, and then calculating the mean of all numerical values of the shortest distance of all PSD95 puncta with Ykt6 puncta.

Synaptosomal Fractionation

Synaptosomal fractionation was performed following a protocol adapted from Bermejo et.al(63). Adult brains were extracted in accordance with Northwestern University administrative panel on laboratory animal care post-decapitation. The brain was chopped with a razor blade and washed with ECS once

before the glycine treatment. The brain was then snap frozen with liquid nitrogen until further processing.

The fractionation was performed as follows: solutions shown in table 1 below were chilled, and HALT protease/phosphatase inhibitor (Thermo Scientific, 78440) was added at 1:100 dilution to all solutions.

All samples and solutions were kept on ice during the procedure. The tissue was placed in a dounce homogenizer along with 1mL of 0.32M HEPES-buffered sucrose solution and homogenized with the motor drive set at 900rpm (setting 7) over 30 second period with 12 strokes. The homogenizer was rinsed with deionized water and wiped dry with Kimwipes in between samples. 10μL of homogenate was preserved and diluted to 4 times the concentration using 0.32M HEPES-buffered sucrose solution, then stored at -80°C for subsequent protein quantification and western blot analysis of the total protein fraction.

The remaining homogenate was centrifuged in a fixed angle rotor at 900xg for 10 minutes at 4°C. The supernatant (S1) was transferred to a clean Eppendorf tube, while the nuclear fraction (P1) was resuspended in 500μL of 0.32M HEPES-buffered sucrose and stored at -80 °C and used for western blot analysis of the nuclear fraction.

S1 was then centrifuged at 10,000xg for 15 minutes at 4°C. The supernatant (S2) was removed and stored at -80 °C. The pellet (P2) was resuspended in 1mL of 0.32M HEPES-buffered sucrose solution and centrifuged at 10,000xg for 15 minutes at 4°C. The supernatant (S2') was removed and stored at -80 °C for subsequent protein quantification and western blot analysis of the cytosolic/light membrane fraction.

The pellet was then lysed by resuspending it in 1mL of ddH_2O, transferred to a glass-Teflon tissue homogenizer, and rapidly homogenized by hand with 3 strokes. The sample was quickly adjusted to 4mM HEPES with 4μL of 1M HEPES solution, then returned to an Eppendorf tube, and the samples were then rotated at 4°C for 30 minutes to complete the lysing.

The sample was then centrifuged at 21,700xg for 24 minutes at 4°C. The supernatant containing the crude vesicular fraction (S3) was stored in -80°C, and the pellet was resuspended in 0.32M HEPES-buffered sucrose solution. The discontinuous sucrose gradient was prepared in 4mL open top thinwall ultra-clear tube (Beckman Coulter, 344062) by layering 1mL each of 1.2M HEPES-buffered sucrose solution, followed by 1.0M HEPES-buffered sucrose solution, then 0.8M HEPES-buffered sucrose solution using a P1000 pipette. Finally, the sample was layered on top, and the tubes were balanced using P200 pipette and adding 0.32M HEPES-buffered sucrose solution onto the top layer. The

samples were then ultracentrifuged for 2 hours at 4°C in swinging buckets (Beckman Coulter, SW-60Ti) using Optima XE-90 ultracentrifuge (Beckman Coulter). Using an 18G needle and a 1mL syringe, the tubes were then punctured at the 1.0M/1.2M HEPES-buffered sucrose solution interphase and the band (synaptic plasma membrane layer, SPM) was withdrawn. The volume was noted, and the collected layer was placed in 3.5mL thickwall ultracentrifuge tubes (Beckman Coulter, 349622) and 2.5 times the volume of SPM of 4mM HEPES was added to adjust the sucrose concentration from 1.2M to 0.32M. The tubes were then balanced with 0.32M HEPES-buffered sucrose solution, and the samples were ultracentrifuged in the swinging bucket rotor at 200,000xg for 30 minutes at 4°C. The supernatant was discarded, and the pellet was resuspended in 100µL of 50mM HEPES/2mM EDTA solution, then stored in -80 °C until used for western blotting.

Western Blot

Protein concentration was analyzed with the Pierce BCA Protein Assay kit (Thermo Scientific, 23225). After the addition of the appropriate amount of the 6X Laemmli Sample Buffer (Bio-rad sab03-02) with 5% ß-mercaptoethanol (Sigma Aldrich, M6250) protein samples were boiled and separated on precast 4-20% Criterion TGX Stain-free gels (Bio-Rad) and transferred to a nitrocellulose membrane (Amersham Protran 0.2 µm NC, #10600001). Membranes were blocked with 3% BSA in 1X Tris-buffered saline (TBS) (50mM Tris/Cl pH 7.4, 150mM NaCl) for 1 hour at room temperature. Membranes were subsequently immunoblotted overnight in primary antibody (anti-Ykt6: 1:100; anti-GAPDH: 1:500; anti-PSD95: 1:1000; anti-GluA1: 1:1000) at 4°C, shaking. The following day, membranes were washed three times with 1X TBST (TBS with 0.1% Tween) for 5 minutes and incubated in secondary IRDye antibody at 1:15000 dilution for 1 hour shaking at room temperature. Membranes were washed three times with 1X TBST for before imaging using Li-Cor Odyssey® CLx Imaging System. Images were processed and quantified using Image Studio Software (LI-COR Biosciences).

Electrophysiology

Mini EPSCs were recorded from infected primary hippocampal cultures in whole-cell voltage clamp. Recordings were performed between DIV 18-21. The external solution contained the following (in mM): 150 NaCl, 2.8 KCl, 2 $CaCl_2$, 1 $MgCl_2$, 10 glucose, and 10 m HEPES (pH adjusted to 7.3 with NaOH), with D-AP5 (50 µM), picrotoxin (50 µM), and tetrodotoxin (1µM) added. The internal solution used in recordings (in mM): 110 CsF, 30 CsCl, 10 Cs-HEPES, 5 EGTA, 4 m NaCl, and 0.5 $CaCl_2$ (pH adjusted to 7.3 with CsOH). Cells were held at −70 mV in voltage clamp with an Axopatch 200B amplifier (Molecular Devices). Data were analyzed with Clampfit version 11.0.3 (Molecular Devices).

Electron Microscopy

Samples were prepared from an adapted protocol by Arai and Waguri (64). 10 minutes at room temperature and 50 minutes at 4°C. Cells were washed with 0.12 M phosphate buffer pH 7.4 and then treated with 1% osmium tetroxide and 1.5% potassium ferrocyanide (Sigma) in 0.12M phosphate buffer pH 7.4. Cells were dehydrated by an ascending series of alcohol (50, 70, 80, 90, and 100%) followed by treatment with epoxy resin for 24 hours. The grids were mounted on resin blocks and cured at 65°C for 3 days. The blocks were trimmed to contain CSMN before proceeding to ultra-thin sectioning. Resin blocks were sectioned on a Leica Ultracut UC6 ultramicrotome (Leica Inc., Nussloch, Germany). Sections (70nm) were collected on 200 mesh copper-palladium grids. Ultra-thin sections were counterstained on a drop of UranyLess solution (Electron Microscopy Sciences, Hatfield, PA) and 0.2% lead citrate. Grids were examined on FEI Tecnai Spirit G2 TEM (FEI Company, Hillsboro, OR) and digital images were captured on an FEI Eagle camera. Post-image acquisition adjustment was performed by Adobe Photoshop 2025.

Circular structures that were between 35 to 45 nm were considered as synaptic vesicles (65) and were manually counted. Those that were touching the membrane were counted as readily releasable pool (RRP), those close to the membrane but not touching were counted as recycling pool, and those distal to the membrane and the synaptic contact points were considered to be the reserve pool. Vesicular size was manually quantified using ImageJ.

Statistical Analysis

Graphpad Prism 10 (http://graphpad.com) was used to graph, organize, and perform all statistical analysis. Statistical analysis was determined using the following methods: in case of more than two conditions, Bartlett's Test was performed to test for homogeneity of variances. If the variances were heterogeneous, one-way analysis of variance (ANOVA) with Welch's correction alongside with Dunnett's T3 multiple comparisons test was performed; otherwise, standard ANOVA with multiple comparison was applied. In cases where two conditions were compared, F-test was performed to compare variances. If the variances were homogeneous, standard T-test was applied; otherwise, T-test with Welch's correction was used to examine the significance of the results.

For the cumulative probability distribution, the event values were binned to construct the cumulative probability, and Kormagorov-Smirnov test was applied to examine whether the distribution differed significantly from each other.

Results

We first began by examining Ykt6 expression in the mammalian brain using the human and mouse brain atlas (66, 67). In the human brain, Ykt6 expression was assayed using two different mRNA probes against Ykt6 in 6 patients. As a reference control, we analysed the expression of the neuronal specific microtubule associated protein 2 (MAP2), a highly expressed neuronal protein. Relative to MAP2, the highest expression of Ykt6 was in the globus pallidus followed by the hippocampus (Figure 1A, hippocampal formation). In the rodent brain, while the mRNA probe for Ykt6 was ubiquitously expressed throughout the brain, its expression was increased in the hippocampus and cerebellum, followed by the frontal cortex (Figure 1B). Together, these data show that Ykt6 is highly expressed in the hippocampus in the mammalian brain, a brain region critically implicated in synucleinopathy-related dementias (68–80).

We next examined the intracellular localization of Ykt6 in hippocampal neurons using immunofluorescence. Under resting conditions, Ykt6 was primarily cytosolic in both the somatic and dendritic regions (Figure 2A, C). Consistent with its role in the secretory pathway (81), Ykt6 also localized to the Golgi apparatus, as shown by the colocalization with the Golgi marker GM130 (Figure 2B, D), and to the ER, as evidenced by the colocalization with the ER-resident protein disulfide isomerase (PDI) (Figure 2F, H). The specificity of the antibody against endogenous Ykt6 was confirmed, as reducing Ykt6 expression with an inducible ShRNA-targeting vector significantly diminished Ykt6 detection by immunofluorescence (Supplemental Figure 2F, H, N, P). Moreover, Ykt6 was also present at postsynaptic terminals and moved closer to synaptic terminals under cLTP conditions, as demonstrated by its colocalization with the postsynaptic marker postsynaptic density protein 95 (PSD95) through immunofluorescence (Figure 2I) and biochemically by subcellular fractionation (Figure J-K). Interestingly, the induction of chemical LTP (cLTP) with glycine, a widely used method to enhance synaptic plasticity at postsynaptic sites (82–87), increased Ykt6 expression at postsynaptic terminals compared to basal conditions (Figure 2K). Together, these data indicate that Ykt6 is associated with the secretory organelles ER and Golgi and can be mobilized to postsynaptic terminals upon cLTP induction.

Modulation of the synaptic distribution of AMPARs underlies synaptic plasticity (53–56). Secretory transport of AMPA receptors may modulate the synaptic pool available for membrane insertion, thereby impacting synaptic plasticity. Among the four AMPARs subunits (GluA1-4), GluA1 is a good candidate for studying secretory transport in relation to synaptic plasticity in hippocampal neurons. In the hippocampus, GluA1A2 heteromers primarily mediate synaptic transmission (88, 89). While GluA2 localizes around the plasma membrane and remains relatively static, GluA1 relieves more on intracellular trafficking for constant transport to the synaptic space. Moreover, the synaptic insertion of

GluA1-containing AMPARs is necessary for LTP (87, 89–98). To test if Ykt6 effects the distribution of endogenous AMPARs, we performed immunocytochemistry for surface and internal GluA1. The surface-to-internal ratio indicates that the regulation primarily occurs at the plasma membrane level rather than reflecting a global change in GluA1 expression. Hippocampal neurons were co-transduced with lentiviruses expressing an inducible ShRNA targeting Ykt6 to knock down its expression, or a scramble ShRNA sequence as a control. Additionally, GFP or GFP-Ykt6 WT, which is resistant to the Ykt6 ShRNA, was co-expressed to rescue Ykt6 expression to endogenous levels (Figure 3). We first confirmed by western blot that human Ykt6 construct does indeed rescue Ykt6 expression to endogenous levels (Figure 3A).

Under resting conditions, Ykt6 knockdown (Sh Ykt6) reduced the surface expression of GluA1 compared to the control (Sh Ctrl) (Figure 3C). This effect was specific to Ykt6, as co-expression of the Ykt6 knockdown-resistant construct (Sh Ykt6 + WT-Ykt6-GFP) restored basal surface GluA1 levels (Figure 3C). Contrary to expectation, overexpression of WT-Ykt6 (Sh Ctrl + WT-Ykt6-GFP) did not increase surface GluA1 levels under basal conditions (Figure 3C), suggesting that GluA1 regulation is tightly controlled at rest.

As expected, under control conditions (Sh Ctrl), cLTP treatment resulted in a two-fold increase in surface expression of GluA1 (Figure 3C, grey bars). On the other hand, Ykt6 knockdown (Sh Ykt6) prevented the increase in GluA1 surface expression upon cLTP (Figure 3C, purple bars). Importantly, this effect was specific to Ykt6, as restoring endogenous Ykt6 expression with the knockdown-resistant construct (Sh Ykt6 + WT-Ykt6-GFP) reinstated the two-fold increase in surface GluA1 levels following cLTP treatment, like the control (Figure 3C, blue bars). While overexpression of WT-Ykt6 (Sh Ctrl + WT-Ykt6-GFP) enhanced surface GluA1 levels compared to control, this effect was not statistically significant (Figure 3C, green bars). Collectively, these findings indicate that Ykt6 regulates both basal and cLTP-dependent surface GluA1 levels.

While the data above suggest that Ykt6 modulates synaptic connections and their downstream effects, we performed whole-cell patch-clamp electrophysiology to measure miniature excitatory post-synaptic currents (mEPSCs) in pyramidal hippocampal neurons to better understand the dynamics of these synaptic connections. Patched neurons were recorded in the presence of NMDA receptor blocker D-2-amino-5-phosphonopentanoic acid (D-APV), voltage-gated sodium channel blocker tetrodotoxin (TTX), and Gamma-Aminobutyric acid (GABA) subunit A ($GABA_A$) receptor antagonist picrotoxin (PTX) to isolate AMPA-mediated currents. Ykt6 knockdown (Sh Ykt6) reduced the amplitude of mEPSCs compared to the control (Sh Ctrl) (Sh Ykt6, 8.728 ± 0.486pA, Sh Ctrl, 10.64 ± 0.400pA, $p = 0.009$, unpaired T-test) (Figure 4B). The observed reduction in mEPSC amplitude aligns

with the decrease in GluA1 surface density at the postsynaptic site (Figure 3B-C). Moreover, we observed a concordant decrease in the interevent cumulative percentage (Figure 3C, $D = 0.595$, $p < 0.0001$) and the frequency of spike intervals in Ykt6 knockdown (Sh Ykt6, 0.357 ± 0.037 Hz) compared to the control (Sh Ctrl, 0.750 ± 0.010 Hz) (Figure 4D, $p = 0.003$, unpaired T-test with Welch's correction). Furthermore, the decrease in mEPSCs is not attributable to neuronal viability issues, as ATP levels – a reliable surrogate for cell viability – were unaffected by Ykt6 knockdown (Figure 4F). Together, these data indicate that GluA1 regulation by Ykt6 affects synapse function of pyramidal hippocampal neurons.

To investigate whether this change was due to the change in synaptic vesicular pool, we performed electron microscopy on the synaptic terminals to quantify the vesicular pools at synaptic contact points for both control and Ykt6 knockdowns. We classified the vesicles that are touching the membranes in the images as readily releasable pool (RRP), those proximal to the contact point but not touching to be the recycling pool, and those distal from the contact point to be the reserve pool. During the search for synaptic contact points, we observed thinner spines in Ykt6 knockdown compared to the control, with depleted postsynaptic densities (Figure 4G). Remarkably, Ykt6 knockdown showed fewer synaptic vesicles in the RRP and the reserve pool, although distal pool remained unaffected (Figures 5H-J). We further observed slightly larger synaptic vesicles on average in the Ykt6 knockdown (Figure 5K).

The secretory pathway supplies proteins and membrane lipids for dendritic morphogenesis (99, 100). Deficits in synaptic function can impact the dendritic arbor (101–104), as neuronal maturity, increased activity, and dendritic elongation and arborization are strongly correlated (97–102). To examine the effect of Ykt6 in dendritic arborization, hippocampal neurons were transduced with Ykt6 knockdown (Sh Ykt6) and control (Sh Ctrl) lentiviruses and immunostained with mCherry at DIV 21 assessed via Sholl analysis by ImageJ (61). Sholl analysis quantifies the number of intersections, which represents branching at varying distances from the soma. Reduced expression of Ykt6 (Sh Ykt6) decreased the dendritic arbor complexity of pyramidal hippocampal neurons compared to the shRNA control (Figure 5B), and the maximum number of intersections occurred more proximal to the soma than the control (Figure 5C). Together, these data suggest that Ykt6 plays a critical role in the regulation of the dendritic arbor.

Discussion

Although most studies on Ykt6 roles in the secretory and autophagy pathways have been conducted in yeast and mammalian systems, its physiological function in the brain remains largely unexplored. Here, we demonstrate that Ykt6 is highly expressed in the hippocampus of the mammalian brain. In

hippocampal pyramidal neurons, Ykt6 is associated with secretory organelles such as the ER and Golgi (105) and can be mobilized to postsynaptic terminals upon cLTP induction. Furthermore, we show that Ykt6 regulates both basal and cLTP-dependent surface GluA1 levels, impacting the dynamics of hippocampal synaptic connections.

Ykt6 is an essential R-SNARE protein with established roles in two key vesicular trafficking pathways: the secretory and autophagy pathways (8, 18, 20, 23–25, 27, 31, 32, 36, 39, 106–109). Our findings suggest a novel role for Ykt6 in regulating AMPARs via the secretory pathway, distinct from its roles in autophagy or exocytosis. This hypothesis is derived from three key lines of previous evidence: 1) regulation by autophagy, 2) SNARE complex formation, and 3) specialized secretory outposts.

While surface expression of AMPARs can be modulated by autophagy in an activity-dependent manner (110–115), autophagy primarily facilitates the degradation of these receptors. In contrast, our data demonstrate that Ykt6 has a positive role in both basal and activity-dependent AMPAR trafficking, enhancing receptor surface expression rather than contributing to their degradation. Downregulation of Ykt6 not only prevents the trafficking of GluA1 to the surface, thereby contributing to the reduction in amplitude, it appears to be contributing to longer IEIs by either preventing vesicles to be incorporated into the readily releasable pools and diminishing the recycling pools as well. This, in turn, is correlated to reduced dendritic arborization (116). The reduction of surface GluA1s may also be attributed to the reduced dendritic spine density, which may also contribute for the increased IEI aside from the reduction in synaptic vesicular pools, thereby reducing the space for AMPARs to occupy (117, 118).

The role of the R-SNARE VAMP2 (Synaptobrevin-2) in forming well-established SNARE complexes, such as SNAP25–Syntaxin-1A/B–VAMP2 or VAMP2–Syntaxin-3–SNAP-47, is critical for exocytosis and endocytosis of AMPARs at postsynaptic terminals (44, 119–124). Although Ykt6, as another R-SNARE, could theoretically substitute for VAMP2 in these complexes, it remains unclear how Ykt6 might displace VAMP2 from its known binding partners.

Neurons have evolved specialized ER and Golgi outposts at distal locations from the soma to enable rapid and precise delivery of protein cargo to synapses (125, 126). Extensive networks of smooth ER tubules and sheets in dendrites and spines suggest local secretory trafficking, bypassing traditional somatic pathways (43, 51, 104, 127–131). ER exit sites (ERES) and COPII subunits have been observed at both proximal and distal dendritic locations in hippocampal neurons (128, 132, 133). Similarly, Golgi outposts in dendritic and axonal compartments support localized secretory functions essential for synaptic plasticity and neuronal responses. These organelles may directly contribute to AMPAR trafficking at synaptic terminals. Furthermore, AMPAR subunit assembly occurs within the ER

(134–137), and recent evidence suggests alternative sources of AMPAR synthesis that are coupled to synaptic plasticity-dependent signals (55, 138, 139). For example, in Drosophila, intra-Golgi transport is regulated by Ca^{2+}-calmodulin-dependent kinase II, an enzyme activated during LTP (40, 140–142). Additionally, local synthesis of AMPARs in dendrites has been observed, bypassing the Golgi and relying instead on the ER-Golgi intermediate compartment (ERGIC) and recycling endosomes (143–145). The dendritic ER also plays a critical role in long-term depression (LTD), a form of synaptic plasticity. During LTD, ER Ca^{2+} release is enhanced, NMDAR trafficking is upregulated, and the ER network near spines becomes more complex (146–149). These findings highlight the importance of the dendritic ER in supporting synaptic plasticity. Understanding how Ykt6 regulates AMPAR secretory trafficking at distal secretory outposts will be crucial for elucidating its molecular mechanisms and functional significance, particularly in the context of neuronal plasticity and synaptic function.

A block in ER-to-Golgi transport and a loss of Ykt6 function is a prominent feature of αSyn pathology across various model systems (8, 18, 20, 34, 150, 151). Previous findings from our laboratory showed that αSyn-dependent ER-to-Golgi trafficking blocks lead to pathological cytosolic Ca^{2+} levels and constitutive activation of calcineurin, resulting in Ykt6 dephosphorylation and loss of function (18). Furthermore, αSyn has been shown to disrupt AMPAR and NMDAR surface levels at synapses, impairing LTP and spatial learning (74, 152–156). Consistent with these findings, we showed that physiologic Ykt6 loss of function in the hippocampus leads to defects in basal and cLTP-dependent GluA1 surface levels. Thus, our data provide a mechanistic explanation for how αSyn disrupts AMPAR trafficking and synaptic plasticity. Defects in AMPAR surface-level regulation have been linked not only to Parkinson's disease but also to other neurodegenerative disorders characterized by cognitive and memory deficits, such as Alzheimer's disease (138, 157–167), as well as a range of neurodevelopmental and psychiatric disorders. Our findings highlight a novel role for Ykt6 in AMPAR regulation in the hippocampus, potentially opening new therapeutic avenues for these devastating conditions.

References

1. Alexander, G. E. (2004) Biology of Parkinson's disease: pathogenesis and pathophysiology of a multisystem neurodegenerative disorder. *Dialogues Clin Neurosci*. **6**, 259–280
2. Armstrong, R. (1998) Lewy body and Alzheimer pathology in temporal lobe in dementia with Lewy bodies. *Alzheimer's Reports*. **1**, 159–163
3. Chin, K. S. (2023) Pathophysiology of dementia
4. Jellinger, K. A. (2024) Behavioral disorders in dementia with Lewy bodies: old and new knowledge. *J Neural Transm*. 10.1007/s00702-024-02823-w
5. Jellinger, K. A., and Korczyn, A. D. (2018) Are dementia with Lewy bodies and Parkinson's disease dementia the same disease? *BMC Medicine*. **16**, 34

6. Kingwell, K. (2017) Zeroing in on neurodegenerative α-synuclein. *Nature Reviews Drug Discovery*. **16**, 371–373
7. Caraveo, G., Auluck, P. K., Whitesell, L., Chung, C. Y., Baru, V., Mosharov, E. V., Yan, X., Ben-Johny, M., Soste, M., Picotti, P., Kim, H., Caldwell, K. A., Caldwell, G. A., Sulzer, D., Yue, D. T., and Lindquist, S. (2014) Calcineurin determines toxic versus beneficial responses to α-synuclein. *Proc Natl Acad Sci U S A*. **111**, E3544-3552
8. Cuddy, L. K., Wani, W. Y., Morella, M. L., Pitcairn, C., Tsutsumi, K., Fredriksen, K., Justman, C. J., Grammatopoulos, T. N., Belur, N. R., Zunke, F., Subramanian, A., Affaneh, A., Lansbury, P. T., and Mazzulli, J. R. (2019) Stress-Induced Cellular Clearance Is Mediated by the SNARE Protein ykt6 and Disrupted by α-Synuclein. *Neuron*. **104**, 869-884.e11
9. Caraveo, G., Soste, M., Cappelleti, V., Fanning, S., van Rossum, D. B., Whitesell, L., Huang, Y., Chung, C. Y., Baru, V., Zaichick, S., Picotti, P., and Lindquist, S. (2017) FKBP12 contributes to α-synuclein toxicity by regulating the calcineurin-dependent phosphoproteome. *Proc Natl Acad Sci U S A*. **114**, E11313–E11322
10. Chawla, S., Ahmadpour, D., Schneider, K. L., Kumar, N., Fischbach, A., Molin, M., and Nystrom, T. (2023) Calcineurin stimulation by Cnb1p overproduction mitigates protein aggregation and α-synuclein toxicity in a yeast model of synucleinopathy. *Cell Communication and Signaling*. **21**, 220
11. Groth, R. D., Dunbar, R. L., and Mermelstein, P. G. (2003) Calcineurin regulation of neuronal plasticity. *Biochemical and Biophysical Research Communications*. **311**, 1159–1171
12. Wu, H.-Y., Tomizawa, K., Oda, Y., Wei, F.-Y., Lu, Y.-F., Matsushita, M., Li, S.-T., Moriwaki, A., and Matsui, H. (2004) Critical Role of Calpain-mediated Cleavage of Calcineurin in Excitotoxic Neurodegeneration *. *Journal of Biological Chemistry*. **279**, 4929–4940
13. Huang, M., Wang, B., Li, X., Fu, C., Wang, C., and Kang, X. (2019) α-Synuclein: A Multifunctional Player in Exocytosis, Endocytosis, and Vesicle Recycling. *Front. Neurosci.* 10.3389/fnins.2019.00028
14. Burré, J. The Synaptic Function of α-Synuclein. *J Parkinsons Dis*. **5**, 699–713
15. Shum, A., Zaichick, S., McElroy, G. S., D'Alessandro, K., Alasady, M. J., Novakovic, M., Peng, W., Grebenik, E. A., Chung, D., Flanagan, M. E., Smith, R., Morales, A., Stumpf, L., McGrath, K., Krainc, D., Mendillo, M. L., Prakriya, M., Chandel, N. S., and Caraveo, G. (2023) Octopamine metabolically reprograms astrocytes to confer neuroprotection against α-synuclein. *Proceedings of the National Academy of Sciences*. **120**, e2217396120
16. Mondal, R., Banerjee, C., Nandy, S., Roy, M., and Chakraborty, J. (2023) Calcineurin inhibition protects against dopamine toxicity and attenuates behavioral decline in a Parkinson's disease model. *Cell & Bioscience*. **13**, 140
17. Wardaszka, P., Soczewka, P., Sienko, M., Zoladek, T., and Kaminska, J. (2021) Partial Inhibition of Calcineurin Activity by Rcn2 as a Potential Remedy for Vps13 Deficiency. *Int J Mol Sci*. **22**, 1193
18. McGrath, K., Agarwal, S., Tonelli, M., Dergai, M., Gaeta, A. L., Shum, A. K., Lacoste, J., Zhang, Y., Wen, W., Chung, D., Wiersum, G., Shevade, A., Zaichick, S., van Rossum, D. B., Shuvalova, L., Savas, J. N., Kuchin, S., Taipale, M., Caldwell, K. A., Caldwell, G. A., Fasshauer, D., and Caraveo, G. (2021) A conformational switch driven by phosphorylation regulates the activity of the evolutionarily conserved SNARE Ykt6. *Proc Natl Acad Sci U S A*. **118**, e2016730118
19. Cooper, A. A., Gitler, A. D., Cashikar, A., Haynes, C. M., Hill, K. J., Bhullar, B., Liu, K., Xu, K., Strathearn, K. E., Liu, F., Cao, S., Caldwell, K. A., Caldwell, G. A., Marsischky, G., Kolodner, R. D., LaBaer, J., Rochet, J.-C., Bonini, N. M., and Lindquist, S. (2006) α-Synuclein Blocks ER-Golgi Traffic and Rab1 Rescues Neuron Loss in Parkinson's Models. *Science*. **313**, 324–328
20. Pitcairn, C., Murata, N., Zalon, A., Stojkovska, I., and Mazzulli, J. R. (2023) Impaired autophagic-lysosomal fusion in Parkinson's patient midbrain neurons occurs through loss of ykt6 and is rescued by farnesyltransferase inhibition. *J Neurosci*. 10.1523/jneurosci.0610-22.2023
21. Malsam, J., and Söllner, T. H. (2011) Organization of SNAREs within the Golgi Stack. *Cold Spring Harb Perspect Biol*. **3**, a005249

22. Ji, J., Yu, Y., Wu, S., Wang, D., Weng, J., and Wang, W. (2023) Different conformational dynamics of SNARE protein Ykt6 among yeast and mammals. *Journal of Biological Chemistry*. 10.1016/j.jbc.2023.104968
23. Matsui, T., Jiang, P., Nakano, S., Sakamaki, Y., Yamamoto, H., and Mizushima, N. (2018) Autophagosomal YKT6 is required for fusion with lysosomes independently of syntaxin 17. *Journal of Cell Biology*. **217**, 2633–2645
24. Gao, J., Reggiori, F., and Ungermann, C. (2018) A novel in vitro assay reveals SNARE topology and the role of Ykt6 in autophagosome fusion with vacuoles. *J Cell Biol*. **217**, 3670–3682
25. Gao, J., Kurre, R., Rose, J., Walter, S., Fröhlich, F., Piehler, J., Reggiori, F., and Ungermann, C. (2020) Function of the SNARE Ykt6 on autophagosomes requires the Dsl1 complex and the Atg1 kinase complex. *EMBO reports*. **21**, e50733
26. Takáts, S., Glatz, G., Szenci, G., Boda, A., Horváth, G. V., Hegedűs, K., Kovács, A. L., and Juhász, G. (2018) Non-canonical role of the SNARE protein Ykt6 in autophagosome-lysosome fusion. *PLoS Genet*. **14**, e1007359
27. Kriegenburg, F., Bas, L., Gao, J., Ungermann, C., and Kraft, C. (2019) The multi-functional SNARE protein Ykt6 in autophagosomal fusion processes. *Cell Cycle*. **18**, 639–651
28. Wen, W., Yu, J., Pan, L., Wei, Z., Weng, J., Wang, W., Ong, Y. S., Tran, T. H. T., Hong, W., and Zhang, M. (2010) Lipid-Induced conformational switch controls fusion activity of longin domain SNARE Ykt6. *Mol Cell*. **37**, 383–395
29. Weng, J., Yang, Y., and Wang, W. (2015) Lipid regulated conformational dynamics of the longin SNARE protein Ykt6 revealed by molecular dynamics simulations. *J Phys Chem A*. **119**, 1554–1562
30. Karuna M, P., Witte, L., Linnemannstoens, K., Choezom, D., Danieli-Mackay, A., Honemann-Capito, M., and Gross, J. C. (2020) Phosphorylation of Ykt6 SNARE Domain Regulates Its Membrane Recruitment and Activity. *Biomolecules*. **10**, 1560
31. McNew, J. A., Søgaard, M., Lampen, N. M., Machida, S., Ye, R. R., Lacomis, L., Tempst, P., Rothman, J. E., and Söllner, T. H. (1997) Ykt6p, a Prenylated SNARE Essential for Endoplasmic Reticulum-Golgi Transport*. *Journal of Biological Chemistry*. **272**, 17776–17783
32. Shirakawa, R., Goto-Ito, S., Goto, K., Wakayama, S., Kubo, H., Sakata, N., Trinh, D. A., Yamagata, A., Sato, Y., Masumoto, H., Cheng, J., Fujimoto, T., Fukai, S., and Horiuchi, H. (2020) A SNARE geranylgeranyltransferase essential for the organization of the Golgi apparatus. *EMBO J*. 10.15252/embj.2019104120
33. Meiringer, C. T. A., Auffarth, K., Hou, H., and Ungermann, C. (2008) Depalmitoylation of Ykt6 Prevents its Entry into the Multivesicular Body Pathway. *Traffic*. **9**, 1510–1521
34. Tsunemi, T., Ishiguro, Y., Yoroisaka, A., Feng, D., Shimada, T., Niiyama, S., Sasazawa, Y., Ishikawa, K., Akamatsu, W., and Hattori, N. (2025) Alpha-synuclein inhibits the secretion of extracellular vesicles through disruptions in YKT6 lipidation. *J. Neurosci.* 10.1523/JNEUROSCI.2350-23.2024
35. Dai, Y., Seeger, M., Weng, J., Song, S., Wang, W., and Tan, Y.-W. (2016) Lipid Regulated Intramolecular Conformational Dynamics of SNARE-Protein Ykt6. *Sci Rep*. **6**, 30282
36. Dietrich, L. E., Gurezka, R., Veit, M., and Ungermann, C. (2004) The SNARE Ykt6 mediates protein palmitoylation during an early stage of homotypic vacuole fusion. *The EMBO Journal*. **23**, 45–53
37. Catchpoole, D. R., and Wanjin, H. (1999) Characterization of the Sequence and Expression of a Ykt6 Prenylated SNARE from Rat. *DNA and Cell Biology*. **18**, 141–145
38. Veit, M. (2004) The human SNARE protein Ykt6 mediates its own palmitoylation at C-terminal cysteine residues. *Biochemical Journal*. **384**, 233–237
39. Hasegawa, H., Zinsser, S., Rhee, Y., Vik-Mo, E. O., Davanger, S., and Hay, J. C. (2003) Mammalian Ykt6 Is a Neuronal SNARE Targeted to a Specialized Compartment by its Profilin-like Amino Terminal Domain. *MBoC*. **14**, 698–720
40. Hanus, C., Kochen, L., Dieck, S. tom, Racine, V., Sibarita, J.-B., Schuman, E. M., and Ehlers, M. D. (2014) Synaptic Control of Secretory Trafficking in Dendrites. *Cell Rep*. **7**, 1771–1778

41. Ehlers, M. D. (2007) Secrets of the Secretory Pathway in Dendrite Growth. *Neuron*. **55**, 686–689
42. Kulik, Y. D., Watson, D. J., Cao, G., Kuwajima, M., and Harris, K. M. (2019) Structural plasticity of dendritic secretory compartments during LTP-induced synaptogenesis. *eLife*. **8**, e46356
43. Horton, A. C., Rácz, B., Monson, E. E., Lin, A. L., Weinberg, R. J., and Ehlers, M. D. (2005) Polarized Secretory Trafficking Directs Cargo for Asymmetric Dendrite Growth and Morphogenesis. *Neuron*. **48**, 757–771
44. Liu, W., Gao, T., Li, N., Shao, S., and Liu, B. (2024) Vesicle fusion and release in neurons under dynamic mechanical equilibrium. *iScience*. **27**, 109793
45. Schmidt, M. R., and Haucke, V. (2007) Recycling endosomes in neuronal membrane traffic. *Biology of the Cell*. **99**, 333–342
46. Blagotinšek Cokan, K., Mavri, M., Rutland, C. S., Glišić, S., Senćanski, M., Vrecl, M., and Kubale, V. (2020) Critical Impact of Different Conserved Endoplasmic Retention Motifs and Dopamine Receptor Interacting Proteins (DRIPs) on Intracellular Localization and Trafficking of the D2 Dopamine Receptor (D2-R) Isoforms. *Biomolecules*. **10**, 1355
47. Hangen, E., Cordelières, F. P., Petersen, J. D., Choquet, D., and Coussen, F. (2018) Neuronal Activity and Intracellular Calcium Levels Regulate Intracellular Transport of Newly Synthesized AMPAR. *Cell Rep*. **24**, 1001-1012.e3
48. Bonnet, C., Charpentier, J., Retailleau, N., Choquet, D., and Coussen, F. Regulation of different phases of AMPA receptor intracellular transport by 4.1N and SAP97. *eLife*. **12**, e85609
49. Hausser, A., and Schlett, K. (2019) Coordination of AMPA receptor trafficking by Rab GTPases. *Small GTPases*. **10**, 419–432
50. Wamsley, J. K. (1992) Transport of receptors. *Mol Neurobiol*. **6**, 313–321
51. Valenzuela, J. I., and Perez, F. (2015) Diversifying the secretory routes in neurons. *Front Neurosci*. **9**, 358
52. Esteves da Silva, M., Adrian, M., Schätzle, P., Lipka, J., Watanabe, T., Cho, S., Futai, K., Wierenga, C. J., Kapitein, L. C., and Hoogenraad, C. C. (2015) Positioning of AMPA Receptor-Containing Endosomes Regulates Synapse Architecture. *Cell Reports*. **13**, 933–943
53. Huganir, R. L., and Nicoll, R. A. (2013) AMPARs and Synaptic Plasticity: The Last 25 Years. *Neuron*. **80**, 704–717
54. Stockwell, I., Watson, J. F., and Greger, I. H. (2024) Tuning synaptic strength by regulation of AMPA glutamate receptor localization. *BioEssays*. **46**, 2400006
55. Diering, G. H., and Huganir, R. L. (2018) The AMPA Receptor Code of Synaptic Plasticity. *Neuron*. **100**, 314–329
56. Wu, Q.-L., Gao, Y., Li, J.-T., Ma, W.-Y., and Chen, N.-H. (2022) The Role of AMPARs Composition and Trafficking in Synaptic Plasticity and Diseases. *Cell Mol Neurobiol*. **42**, 2489–2504
57. Makino, H., and Malinow, R. (2009) AMPA receptor incorporation into synapses during LTP: the role of lateral movement and exocytosis. *Neuron*. **64**, 381–390
58. Yang, Y., Wang, X., Frerking, M., and Zhou, Q. (2008) Delivery of AMPA receptors to perisynaptic sites precedes the full expression of long-term potentiation. *Proceedings of the National Academy of Sciences*. **105**, 11388–11393
59. Chiu, A. M., Barse, L., Hubalkova, P., and Sanz-Clemente, A. (2019) An Antibody Feeding Approach to Study Glutamate Receptor Trafficking in Dissociated Primary Hippocampal Cultures. *J Vis Exp*. 10.3791/59982
60. Ferreira, T. A., Blackman, A. V., Oyrer, J., Jayabal, S., Chung, A. J., Watt, A. J., Sjöström, P. J., and van Meyel, D. J. (2014) Neuronal morphometry directly from bitmap images. *Nat Methods*. **11**, 982–984
61. Schneider, C. A., Rasband, W. S., and Eliceiri, K. W. (2012) NIH Image to ImageJ: 25 years of image analysis. *Nat Methods*. **9**, 671–675
62. McCall, A. D. (2024) Colocalization by cross-correlation, a new method of colocalization suited for super-resolution microscopy. *BMC Bioinformatics*. **25**, 55

63. Bermejo, M. K., Milenkovic, M., Salahpour, A., and Ramsey, A. J. (2014) Preparation of Synaptic Plasma Membrane and Postsynaptic Density Proteins Using a Discontinuous Sucrose Gradient. *J Vis Exp*. 10.3791/51896
64. Arai, R., and Waguri, S. (2019) Improved Electron Microscopy Fixation Methods for Tracking Autophagy-Associated Membranes in Cultured Mammalian Cells. *Methods Mol Biol*. **1880**, 211–221
65. Südhof, T. C. (1999) Composition of Synaptic Vesicles. in *Basic Neurochemistry: Molecular, Cellular and Medical Aspects. 6th edition*, Lippincott-Raven, [online] https://www.ncbi.nlm.nih.gov/books/NBK28154/ (Accessed February 8, 2025)
66. Allen Institute for Brain Science (2004) Allen Brain Cell Atlas - brain-map.org. [online] https://portal.brain-map.org/atlases-and-data/bkp/abc-atlas (Accessed October 30, 2023)
67. Shen, E. H., Overly, C. C., and Jones, A. R. (2012) The Allen Human Brain Atlas: Comprehensive gene expression mapping of the human brain. *Trends in Neurosciences*. **35**, 711–714
68. Adamowicz, D. H., Roy, S., Salmon, D. P., Galasko, D. R., Hansen, L. A., Masliah, E., and Gage, F. H. (2017) Hippocampal α-Synuclein in Dementia with Lewy Bodies Contributes to Memory Impairment and Is Consistent with Spread of Pathology. *J Neurosci*. **37**, 1675–1684
69. Kasongo, D. W., de Leo, G., Vicario, N., Leanza, G., and Legname, G. (2020) Chronic α-Synuclein Accumulation in Rat Hippocampus Induces Lewy Bodies Formation and Specific Cognitive Impairments. *eNeuro*. **7**, ENEURO.0009-20.2020
70. Koss, D. J., Erskine, D., Porter, A., Palmoski, P., Menon, H., Todd, O. G. J., Leite, M., Attems, J., and Outeiro, T. F. (2022) Nuclear alpha-synuclein is present in the human brain and is modified in dementia with Lewy bodies. *Acta Neuropathologica Communications*. **10**, 98
71. Teil, M., Dovero, S., Bourdenx, M., Arotcarena, M.-L., Darricau, M., Porras, G., Thiolat, M.-L., Trigo-Damas, I., Perier, C., Estrada, C., Garcia-Carrillo, N., Herrero, M. T., Vila, M., Obeso, J. A., Bezard, E., and Dehay, B. (2023) Cortical Lewy body injections induce long-distance pathogenic alterations in the non-human primate brain. *npj Parkinsons Dis.* **9**, 1–13
72. Wirdefeldt, K., Bogdanovic, N., Westerberg, L., Payami, H., Schalling, M., and Murdoch, G. (2001) Expression of α-synuclein in the human brain: relation to Lewy body disease. *Molecular Brain Research*. **92**, 58–65
73. Altay, M. F., Liu, A. K. L., Holton, J. L., Parkkinen, L., and Lashuel, H. A. (2022) Prominent astrocytic alpha-synuclein pathology with unique post-translational modification signatures unveiled across Lewy body disorders. *Acta Neuropathologica Communications*. **10**, 163
74. Dues, D. J., Nguyen, A. P. T., Becker, K., Ma, J., and Moore, D. J. (2023) Hippocampal subfield vulnerability to α-synuclein pathology precedes neurodegeneration and cognitive dysfunction. *npj Parkinsons Dis.* **9**, 1–11
75. Hashimoto, M., and Masliah, E. (2006) Alpha-synuclein in Lewy Body Disease and Alzheimer's Disease. *Brain Pathol*. **9**, 707–720
76. Marotta, N. P., Ara, J., Uemura, N., Lougee, M. G., Meymand, E. S., Zhang, B., Petersson, E. J., Trojanowski, J. Q., and Lee, V. M.-Y. (2021) Alpha-synuclein from patient Lewy bodies exhibits distinct pathological activity that can be propagated in vitro. *Acta Neuropathologica Communications*. **9**, 188
77. Sanderson, J. B., De, S., Jiang, H., Rovere, M., Jin, M., Zaccagnini, L., Hays Watson, A., De Boni, L., Lagomarsino, V. N., Young-Pearse, T. L., Liu, X., Pochapsky, T. C., Hyman, B. T., Dickson, D. W., Klenerman, D., Selkoe, D. J., and Bartels, T. (2020) Analysis of α-synuclein species enriched from cerebral cortex of humans with sporadic dementia with Lewy bodies. *Brain Communications*. **2**, fcaa010
78. Lippa, C. F., Fujiwara, H., Mann, D. M. A., Giasson, B., Baba, M., Schmidt, M. L., Nee, L. E., O'Connell, B., Pollen, D. A., St. George-Hyslop, P., Ghetti, B., Nochlin, D., Bird, T. D., Cairns, N. J., Lee, V. M.-Y., Iwatsubo, T., and Trojanowski, J. Q. (1998) Lewy Bodies Contain Altered α-Synuclein in Brains of Many Familial Alzheimer's Disease Patients with Mutations in Presenilin and Amyloid Precursor Protein Genes. *The American Journal of Pathology*. **153**, 1365–1370

79. Lippa, C. F., Duda, J. E., Grossman, M., Hurtig, H. I., Aarsland, D., Boeve, B. F., Brooks, D. J., Dickson, D. W., Dubois, B., Emre, M., Fahn, S., Farmer, J. M., Galasko, D., Galvin, J. E., Goetz, C. G., Growdon, J. H., Gwinn-Hardy, K. A., Hardy, J., Heutink, P., Iwatsubo, T., Kosaka, K., Lee, V. M.-Y., Leverenz, J. B., Masliah, E., McKeith, I. G., Nussbaum, R. L., Olanow, C. W., Ravina, B. M., Singleton, A. B., Tanner, C. M., Trojanowski, J. Q., and Wszolek, Z. K. (2007) DLB and PDD boundary issues: Diagnosis, treatment, molecular pathology, and biomarkers. *Neurology*. **68**, 812–819
80. Colom-Cadena, M., Pegueroles, J., Herrmann, A. G., Henstridge, C. M., Muñoz, L., Querol-Vilaseca, M., Martín-Paniello, C. S., Luque-Cabecerans, J., Clarimon, J., Belbin, O., Núñez-Llaves, R., Blesa, R., Smith, C., McKenzie, C.-A., Frosch, M. P., Roe, A., Fortea, J., Andilla, J., Loza-Alvarez, P., Gelpi, E., Hyman, B. T., Spires-Jones, T. L., and Lleó, A. (2017) Synaptic phosphorylated α-synuclein in dementia with Lewy bodies. *Brain*. **140**, 3204–3214
81. Zhang, T., and Hong, W. (2001) Ykt6 Forms a SNARE Complex with Syntaxin 5, GS28, and Bet1 and Participates in a Late Stage in Endoplasmic Reticulum-Golgi Transport*. *Journal of Biological Chemistry*. **276**, 27480–27487
82. Stewart, M. G., Medvedev, N. I., Popov, V. I., Schoepfer, R., Davies, H. A., Murphy, K., Dallérac, G. M., Kraev, I. V., and Rodríguez, J. J. (2005) Chemically induced long-term potentiation increases the number of perforated and complex postsynaptic densities but does not alter dendritic spine volume in CA1 of adult mouse hippocampal slices. *Eur J Neurosci*. **21**, 3368–3378
83. Fortin, D. A., Davare, M. A., Srivastava, T., Brady, J. D., Nygaard, S., Derkach, V. A., and Soderling, T. R. (2010) Long-Term Potentiation-Dependent Spine Enlargement Requires Synaptic Ca2+-Permeable AMPA Receptors Recruited by CaM-Kinase I. *J Neurosci*. **30**, 11565–11575
84. Divakaruni, S. S., Van Dyke, A. M., Chandra, R., LeGates, T. A., Contreras, M., Dharmasri, P. A., Higgs, H. N., Lobo, M. K., Thompson, S. M., and Blanpied, T. A. (2018) Long-Term Potentiation Requires a Rapid Burst of Dendritic Mitochondrial Fission during Induction. *Neuron*. **100**, 860-875.e7
85. Fujii, S., Sasaki, H., Mikoshiba, K., Kuroda, Y., Yamazaki, Y., Mostafa Taufiq, A., and Kato, H. (2004) A chemical LTP induced by co-activation of metabotropic and *N*-methyl-d-aspartate glutamate receptors in hippocampal CA1 neurons. *Brain Research*. **999**, 20–28
86. Jin, C., Jang, S.-S., Ge, P., Chung, H. J., and Selvin, P. (2021) Single molecule tracking of AMPA receptors shows the role of synaptic insertion during maintenance of chemical LTP. 10.1101/2021.02.04.429665
87. Lu, W.-Y., Man, H.-Y., Ju, W., Trimble, W. S., MacDonald, J. F., and Wang, Y. T. (2001) Activation of Synaptic NMDA Receptors Induces Membrane Insertion of New AMPA Receptors and LTP in Cultured Hippocampal Neurons. *Neuron*. **29**, 243–254
88. Lu, W., Shi, Y., Jackson, A. C., Bjorgan, K., During, M. J., Sprengel, R., Seeburg, P. H., and Nicoll, R. A. (2009) Subunit composition of synaptic AMPA receptors revealed by a single-cell genetic approach. *Neuron*. **62**, 254–268
89. Shi, S.-H., Hayashi, Y., Esteban, J. A., and Malinow, R. (2001) Subunit-specific rules governing AMPA receptor trafficking to synapses in hippocampal pyramidal neurons. *Cell*. **105**, 331–343
90. Yang, X., Gong, R., Qin, L., Bao, Y., Fu, Y., Gao, S., Yang, H., Ni, J., Yuan, T.-F., and Lu, W. (2022) Trafficking of NMDA receptors is essential for hippocampal synaptic plasticity and memory consolidation. *Cell Reports*. 10.1016/j.celrep.2022.111217
91. Sumi, T., and Harada, K. (2020) Mechanism underlying hippocampal long-term potentiation and depression based on competition between endocytosis and exocytosis of AMPA receptors. *Sci Rep*. **10**, 14711
92. Lüscher, C., Xia, H., Beattie, E. C., Carroll, R. C., von Zastrow, M., Malenka, R. C., and Nicoll, R. A. (1999) Role of AMPA receptor cycling in synaptic transmission and plasticity. *Neuron*. **24**, 649–658

93. Kullmann, D. M., Erdemli, G., and Asztély, F. (1996) LTP of AMPA and NMDA receptor-mediated signals: evidence for presynaptic expression and extrasynaptic glutamate spill-over. *Neuron*. **17**, 461–474
94. Lin, D.-T., Makino, Y., Sharma, K., Hayashi, T., Neve, R., Takamiya, K., and Huganir, R. L. (2009) Regulation of AMPA receptor extrasynaptic insertion by 4.1N, phosphorylation and palmitoylation. *Nat Neurosci*. **12**, 879–887
95. Jensen, V., Kaiser, K. M. M., Borchardt, T., Adelmann, G., Rozov, A., Burnashev, N., Brix, C., Frotscher, M., Andersen, P., Hvalby, Ø., Sakmann, B., Seeburg, P. H., and Sprengel, R. (2003) A juvenile form of postsynaptic hippocampal long-term potentiation in mice deficient for the AMPA receptor subunit GluR-A. *J Physiol*. **553**, 843–856
96. Zamanillo, D., Sprengel, R., Hvalby, Ø., Jensen, V., Burnashev, N., Rozov, A., Kaiser, K. M. M., Köster, H. J., Borchardt, T., Worley, P., Lübke, J., Frotscher, M., Kelly, P. H., Sommer, B., Andersen, P., Seeburg, P. H., and Sakmann, B. (1999) Importance of AMPA Receptors for Hippocampal Synaptic Plasticity But Not for Spatial Learning. *Science*. **284**, 1805–1811
97. Boehm, J., Kang, M.-G., Johnson, R. C., Esteban, J., Huganir, R. L., and Malinow, R. (2006) Synaptic incorporation of AMPA receptors during LTP is controlled by a PKC phosphorylation site on GluR1. *Neuron*. **51**, 213–225
98. Mack, V., Burnashev, N., Kaiser, K. M., Rozov, A., Jensen, V., Hvalby, O., Seeburg, P. H., Sakmann, B., and Sprengel, R. (2001) Conditional restoration of hippocampal synaptic potentiation in Glur-A-deficient mice. *Science*. **292**, 2501–2504
99. Meltzer, S., Bagley, J. A., Perez, G. L., O'Brien, C. E., DeVault, L., Guo, Y., Jan, L. Y., and Jan, Y.-N. (2017) Phospholipid homeostasis regulates dendrite morphogenesis in Drosophila sensory neurons. *Cell Rep*. **21**, 859–866
100. Chen, M., Xu, L., Wu, Y., Soba, P., and Hu, C. (2023) The organization and function of the Golgi apparatus in dendrite development and neurological disorders. *Genes & Diseases*. **10**, 2425–2442
101. Peng, Y.-R., He, S., Marie, H., Zeng, S.-Y., Ma, J., Tan, Z.-J., Lee, S. Y., Malenka, R. C., and Yu, X. (2009) Coordinated changes in dendritic arborization and synaptic strength during neural circuit development. *Neuron*. **61**, 71–84
102. Kirchner, J. H., Euler, L., Fritz, I., Castro, A. F., and Gjorgjieva, J. (2024) Dendritic growth and synaptic organization from activity-independent cues and local activity-dependent plasticity. *eLife*. 10.7554/eLife.87527.2
103. Wen, Q., Stepanyants, A., Elston, G. N., Grosberg, A. Y., and Chklovskii, D. B. (2009) Maximization of the connectivity repertoire as a statistical principle governing the shapes of dendritic arbors. *Proceedings of the National Academy of Sciences*. **106**, 12536–12541
104. Jan, Y.-N., and Jan, L. Y. (2010) Branching out: mechanisms of dendritic arborization. *Nat Rev Neurosci*. **11**, 316–328
105. Tai, G., Lu, L., Wang, T. L., Tang, B. L., Goud, B., Johannes, L., and Hong, W. (2004) Participation of the Syntaxin 5/Ykt6/GS28/GS15 SNARE Complex in Transport from the Early/Recycling Endosome to the Trans-Golgi Network. *Mol Biol Cell*. **15**, 4011–4022
106. Tian, X., Teng, J., and Chen, J. (2021) New insights regarding SNARE proteins in autophagosome-lysosome fusion. *Autophagy*. **17**, 2680–2688
107. Sakata, N., Shirakawa, R., Goto, K., Trinh, D. A., and Horiuchi, H. (2021) Double prenylation of SNARE protein Ykt6 is required for lysosomal hydrolase trafficking. *The Journal of Biochemistry*. **169**, 363–370
108. Yong, C. Q. Y., and Tang, B. L. (2019) Another longin SNARE for autophagosome-lysosome fusion-how does Ykt6 work? *Autophagy*. **15**, 352–357
109. Lee, C., Lepore, D., Lee, S.-H., Kim, T. G., Buwa, N., Lee, J., Munson, M., and Yoon, T.-Y. (2024) Exocyst stimulates multiple steps of exocytic SNARE complex assembly and vesicle fusion. *Nat Struct Mol Biol*. 10.1038/s41594-024-01388-2
110. Overhoff, M., Tellkamp, F., Hess, S., Tutas, J., Tolve, M., Faerfers, M., Ickert, L., Mohammadi, M., Bruyckere, E. D., Kallergi, E., Vedove, A. D., Nikoletopoulou, V., Wirth, B., Isensee, J.,

Hucho, T., Puchkov, D., Isbrandt, D., Krüger, M., Kloppenburg, P., and Kononenko, N. L. (2022) Autophagy regulates neuronal excitability by controlling cAMP/Protein Kinase A signaling. 10.1101/2022.02.11.480034
111. Shehata, M., Abdou, K., Choko, K., Matsuo, M., Nishizono, H., and Inokuchi, K. (2018) Autophagy Enhances Memory Erasure through Synaptic Destabilization. *J. Neurosci.* **38**, 3809–3822
112. Shehata, M., Matsumura, H., Okubo-Suzuki, R., Ohkawa, N., and Inokuchi, K. (2012) Neuronal Stimulation Induces Autophagy in Hippocampal Neurons That Is Involved in AMPA Receptor Degradation after Chemical Long-Term Depression. *Journal of Neuroscience*. **32**, 10413–10422
113. Goo, M. S., Sancho, L., Slepak, N., Boassa, D., Deerinck, T. J., Ellisman, M. H., Bloodgood, B. L., and Patrick, G. N. (2017) Activity-dependent trafficking of lysosomes in dendrites and dendritic spines. *Journal of Cell Biology*. **216**, 2499–2513
114. Hanley, J. G. (2018) The Regulation of AMPA Receptor Endocytosis by Dynamic Protein-Protein Interactions. *Front. Cell. Neurosci.* 10.3389/fncel.2018.00362
115. Lin, J. W., Ju, W., Foster, K., Lee, S. H., Ahmadian, G., Wyszynski, M., Wang, Y. T., and Sheng, M. (2000) Distinct molecular mechanisms and divergent endocytotic pathways of AMPA receptor internalization. *Nature Neuroscience*. **3**, 1282–1290
116. Ratliff, W. A., Delic, V., Pick, C. G., and Citron, B. A. (2020) Dendritic arbor complexity and spine density changes after repetitive mild traumatic brain injury and neuroprotective treatments. *Brain Res*. **1746**, 147019
117. Hsieh, H., Boehm, J., Sato, C., Iwatsubo, T., Tomita, T., Sisodia, S., and Malinow, R. (2006) AMPA-R Removal Underlies Aβ-induced Synaptic Depression and Dendritic Spine Loss. *Neuron*. **52**, 831–843
118. Turrigiano, G. G., and Nelson, S. B. (2004) Homeostatic plasticity in the developing nervous system. *Nat Rev Neurosci*. **5**, 97–107
119. Hong, W. (2005) SNAREs and traffic. *Biochimica et Biophysica Acta (BBA) - Molecular Cell Research*. **1744**, 120–144
120. Jurado, S. (2014) The dendritic SNARE fusion machinery involved in AMPARs insertion during long-term potentiation. *Front. Cell. Neurosci.* 10.3389/fncel.2014.00407
121. Kuster, A., Nola, S., Dingli, F., Vacca, B., Gauchy, C., Beaujouan, J.-C., Nunez, M., Moncion, T., Loew, D., Formstecher, E., Galli, T., and Proux-Gillardeaux, V. (2015) The Q-soluble N-Ethylmaleimide-sensitive Factor Attachment Protein Receptor (Q-SNARE) SNAP-47 Regulates Trafficking of Selected Vesicle-associated Membrane Proteins (VAMPs). *J Biol Chem*. **290**, 28056–28069
122. Urbina, F. L., Menon, S., Goldfarb, D., Edwards, R., Ben Major, M., Brennwald, P., and Gupton, S. L. (2021) TRIM67 regulates exocytic mode and neuronal morphogenesis via SNAP47. *Cell Reports*. **34**, 108743
123. Holt, M., Varoqueaux, F., Wiederhold, K., Takamori, S., Urlaub, H., Fasshauer, D., and Jahn, R. (2006) Identification of SNAP-47, a Novel Qbc-SNARE with Ubiquitous Expression *. *Journal of Biological Chemistry*. **281**, 17076–17083
124. Yan, C., Jiang, J., Yang, Y., Geng, X., and Dong, W. (2022) The function of VAMP2 in mediating membrane fusion: An overview. *Front. Mol. Neurosci.* 10.3389/fnmol.2022.948160
125. Alvarez-Castelao, B., and Schuman, E. M. (2015) The Regulation of Synaptic Protein Turnover. *J Biol Chem*. **290**, 28623–28630
126. Steward, O., and Schuman, E. M. (2003) Compartmentalized synthesis and degradation of proteins in neurons. *Neuron*. **40**, 347–359
127. Bollmann, C., Schöning, S., Kotschnew, K., Grosse, J., Heitzig, N., and Fischer von Mollard, G. (2022) Primary neurons lacking the SNAREs vti1a and vti1b show altered neuronal development. *Neural Dev*. **17**, 12
128. Kemal, S., Richardson, H. S., Dyne, E. D., and Fu, M. (2022) ER and Golgi trafficking in axons, dendrites, and glial processes. *Current Opinion in Cell Biology*. **78**, 102119

129. Evans, A. J., Gurung, S., Wilkinson, K. A., Stephens, D. J., and Henley, J. M. (2017) Assembly, Secretory Pathway Trafficking, and Surface Delivery of Kainate Receptors Is Regulated by Neuronal Activity. *Cell Reports*. **19**, 2613–2626
130. Hanus, C., and Ehlers, M. D. (2008) Secretory outposts for the local processing of membrane cargo in neuronal dendrites. *Traffic*. **9**, 1437–1445
131. Bowen, A. B., Bourke, A. M., Hiester, B. G., Hanus, C., and Kennedy, M. J. (2017) Golgi-independent secretory trafficking through recycling endosomes in neuronal dendrites and spines. *eLife*. **6**, e27362
132. Aridor, M., Guzik, A. K., Bielli, A., and Fish, K. N. (2004) Endoplasmic Reticulum Export Site Formation and Function in Dendrites. *J Neurosci*. **24**, 3770–3776
133. Pick, J. E., and Ziff, E. B. (2018) Regulation of AMPA Receptor Trafficking and Exit from the Endoplasmic Reticulum. *Mol Cell Neurosci*. **91**, 3–9
134. Brechet, A., Buchert, R., Schwenk, J., Boudkkazi, S., Zolles, G., Siquier-Pernet, K., Schaber, I., Bildl, W., Saadi, A., Bole-Feysot, C., Nitschke, P., Reis, A., Sticht, H., Al-Sanna'a, N., Rolfs, A., Kulik, A., Schulte, U., Colleaux, L., Abou Jamra, R., and Fakler, B. (2017) AMPA-receptor specific biogenesis complexes control synaptic transmission and intellectual ability. *Nat Commun*. **8**, 15910
135. Schwenk, J., and Fakler, B. (2021) Building of AMPA-type glutamate receptors in the endoplasmic reticulum and its implication for excitatory neurotransmission. *The Journal of Physiology*. **599**, 2639–2653
136. Penn, A. C., Williams, S. R., and Greger, I. H. (2008) Gating motions underlie AMPA receptor secretion from the endoplasmic reticulum. *The EMBO Journal*. **27**, 3056–3068
137. Morise, J., Suzuki, K. G. N., Kitagawa, A., Wakazono, Y., Takamiya, K., Tsunoyama, T. A., Nemoto, Y. L., Takematsu, H., Kusumi, A., and Oka, S. (2019) AMPA receptors in the synapse turnover by monomer diffusion. *Nat Commun*. **10**, 5245
138. Henley, J. M., and Wilkinson, K. A. (2013) AMPA receptor trafficking and the mechanisms underlying synaptic plasticity and cognitive aging. *Dialogues Clin Neurosci*. **15**, 11–27
139. Govind, A. P., Jeyifous, O., Russell, T. A., Yi, Z., Weigel, A. V., Ramaprasad, A., Newell, L., Ramos, W., Valbuena, F. M., Casler, J. C., Yan, J.-Z., Glick, B. S., Swanson, G. T., Lippincott-Schwartz, J., and Green, W. N. (2021) Activity-dependent Golgi satellite formation in dendrites reshapes the neuronal surface glycoproteome. *eLife*. **10**, e68910
140. Kennedy, G., Gibson, O., T. O'Hare, D., Mills, I. G., and Evergren, E. (2023) The role of CaMKK2 in Golgi-associated vesicle trafficking. *Biochem Soc Trans*. **51**, 331–342
141. Wang, Z., Palmer, G., and Griffith, L. C. (1998) Regulation of Drosophila Ca2+/calmodulin-dependent protein kinase II by autophosphorylation analyzed by site-directed mutagenesis. *J Neurochem*. **71**, 378–387
142. Mikhaylova, M., Hradsky, J., and Kreutz, M. R. (2011) Between promiscuity and specificity: novel roles of EF-hand calcium sensors in neuronal Ca2+ signalling. *Journal of Neurochemistry*. **118**, 695–713
143. Grochowska, K. M., Andres-Alonso, M., Karpova, A., and Kreutz, M. R. (2022) The needs of a synapse—How local organelles serve synaptic proteostasis. *The EMBO Journal*. 10.15252/embj.2021110057
144. O'Sullivan, M. J., and Lindsay, A. J. (2020) The Endosomal Recycling Pathway—At the Crossroads of the Cell. *Int J Mol Sci*. **21**, 6074
145. John Jacob Peters, Leitz, J., Oses-Prieto, J. A., Burlingame, A. L., and Brunger, A. T. (2021) Molecular Characterization of AMPA-Receptor-Containing Vesicles. *Frontiers in Molecular Neuroscience*. 10.3389/fnmol.2021.754631
146. Arias-Cavieres, A., Barrientos, G. C., Sánchez, G., Elgueta, C., Muñoz, P., and Hidalgo, C. (2018) Ryanodine Receptor-Mediated Calcium Release Has a Key Role in Hippocampal LTD Induction. *Front Cell Neurosci*. **12**, 403

147. Miyata, M., Finch, E. A., Khiroug, L., Hashimoto, K., Hayasaka, S., Oda, S.-I., Inouye, M., Takagishi, Y., Augustine, G. J., and Kano, M. (2000) Local Calcium Release in Dendritic Spines Required for Long-Term Synaptic Depression. *Neuron*. **28**, 233–244
148. Baker, K. D., Edwards, T. M., and Rickard, N. S. (2013) The role of intracellular calcium stores in synaptic plasticity and memory consolidation. *Neurosci Biobehav Rev*. **37**, 1211–1239
149. Rose, C. R., and Konnerth, A. (2001) Stores not just for storage. intracellular calcium release and synaptic plasticity. *Neuron*. **31**, 519–522
150. Thayanidhi, N., Helm, J. R., Nycz, D. C., Bentley, M., Liang, Y., and Hay, J. C. (2010) α-Synuclein Delays Endoplasmic Reticulum (ER)-to-Golgi Transport in Mammalian Cells by Antagonizing ER/Golgi SNAREs. *MBoC*. **21**, 1850–1863
151. Caraveo, G., Soste, M., Cappelleti, V., Fanning, S., van Rossum, D. B., Whitesell, L., Huang, Y., Chung, C. Y., Baru, V., Zaichick, S., Picotti, P., and Lindquist, S. (2017) FKBP12 contributes to α-synuclein toxicity by regulating the calcineurin-dependent phosphoproteome. *Proc Natl Acad Sci U S A*. **114**, E11313–E11322
152. Calabresi, P., Di Lazzaro, G., Marino, G., Campanelli, F., and Ghiglieri, V. (2023) Advances in understanding the function of alpha-synuclein: implications for Parkinson's disease. *Brain*. **146**, 3587–3597
153. Diógenes, M. J., Dias, R. B., Rombo, D. M., Miranda, H. V., Maiolino, F., Guerreiro, P., Näsström, T., Franquelim, H. G., Oliveira, L. M. A., Castanho, M. A. R. B., Lannfelt, L., Bergström, J., Ingelsson, M., Quintas, A., Sebastião, A. M., Lopes, L. V., and Outeiro, T. F. (2012) Extracellular Alpha-Synuclein Oligomers Modulate Synaptic Transmission and Impair LTP Via NMDA-Receptor Activation. *J. Neurosci.* **32**, 11750–11762
154. Ghiglieri, V., Calabrese, V., and Calabresi, P. (2018) Alpha-Synuclein: From Early Synaptic Dysfunction to Neurodegeneration. *Front. Neurol.* 10.3389/fneur.2018.00295
155. Sharma, M., and Burré, J. (2023) α-Synuclein in synaptic function and dysfunction. *Trends in Neurosciences*. **46**, 153–166
156. Kulkarni, A. S., Burns, M. R., Brundin, P., and Wesson, D. W. (2022) Linking α-synuclein-induced synaptopathy and neural network dysfunction in early Parkinson's disease. *Brain Communications*. **4**, fcac165
157. Jurado, S. (2018) AMPA Receptor Trafficking in Natural and Pathological Aging. *Front Mol Neurosci*. **10**, 446
158. da Silva, J. A. C., and Schröder, N. (2023) The Role of Ca2+ Permeable AMPA Receptors in Neurodegeneration, Neurotoxicity, and Neuroinflammation. *CNS Neurol Disord Drug Targets*. **22**, 624–633
159. Wright, A. L., Konen, L. M., Mockett, B. G., Morris, G. P., Singh, A., Burbano, L. E., Milham, L., Hoang, M., Zinn, R., Chesworth, R., Tan, R. P., Royle, G. A., Clark, I., Petrou, S., Abraham, W. C., and Vissel, B. (2023) The Q/R editing site of AMPA receptor GluA2 subunit acts as an epigenetic switch regulating dendritic spines, neurodegeneration and cognitive deficits in Alzheimer's disease. *Molecular Neurodegeneration*. **18**, 65
160. Zhang, H., and Bramham, C. R. (2020) Bidirectional Dysregulation of AMPA Receptor-Mediated Synaptic Transmission and Plasticity in Brain Disorders. *Front. Synaptic Neurosci.* 10.3389/fnsyn.2020.00026
161. Kwak, S., and Weiss, J. H. (2006) Calcium-permeable AMPA channels in neurodegenerative disease and ischemia. *Current Opinion in Neurobiology*. **16**, 281–287
162. Guo, C., and Ma, Y.-Y. (2021) Calcium Permeable-AMPA Receptors and Excitotoxicity in Neurological Disorders. *Front. Neural Circuits*. 10.3389/fncir.2021.711564
163. Italia, M., Ferrari, E., Di Luca, M., and Gardoni, F. (2021) GluA3-containing AMPA receptors: From physiology to synaptic dysfunction in brain disorders. *Neurobiology of Disease*. **161**, 105539
164. Feldmeyer, D., Kask, K., Brusa, R., Kornau, H.-C., Kolhekar, R., Rozov, A., Burnashev, N., Jensen, V., Hvalby, Ø., Sprengel, R., and Seeburg, P. H. (1999) Neurological dysfunctions in

mice expressing different levels of the Q/R site–unedited AMPAR subunit GluR–B. *Nat Neurosci*. **2**, 57–64
165. Hettinger, J. C., Lee, H., Bu, G., Holtzman, D. M., and Cirrito, J. R. (2018) AMPA-ergic regulation of amyloid-β levels in an Alzheimer's disease mouse model. *Molecular Neurodegeneration*. **13**, 22
166. Lu, K., Li, C., Liu, J., Wang, J., Li, Y., He, B., Li, J., Zhang, X., Wei, M., Tian, Y., Zhang, R., Zhang, C., and Zhang, Y. (2023) Impairments in endogenous AMPA receptor dynamics correlates with learning deficits in Alzheimer's disease model mice. *Proceedings of the National Academy of Sciences*. **120**, e2303878120
167. Bennett, M. V. L., Pellegrini-Giampietro, D. E., Gorter, J. A., Aronica, E., Connor, J. A., and Zukin, R. S. (1996) The GluR2 Hypothesis: Ca++-permeable AMPA Receptors in Delayed Neurodegeneration. *Cold Spring Harb Symp Quant Biol*. **61**, 373–384
168. Hawrylycz, M. J., Lein, E. S., Guillozet-Bongaarts, A. L., Shen, E. H., Ng, L., Miller, J. A., van de Lagemaat, L. N., Smith, K. A., Ebbert, A., Riley, Z. L., Abajian, C., Beckmann, C. F., Bernard, A., Bertagnolli, D., Boe, A. F., Cartagena, P. M., Chakravarty, M. M., Chapin, M., Chong, J., Dalley, R. A., David Daly, B., Dang, C., Datta, S., Dee, N., Dolbeare, T. A., Faber, V., Feng, D., Fowler, D. R., Goldy, J., Gregor, B. W., Haradon, Z., Haynor, D. R., Hohmann, J. G., Horvath, S., Howard, R. E., Jeromin, A., Jochim, J. M., Kinnunen, M., Lau, C., Lazarz, E. T., Lee, C., Lemon, T. A., Li, L., Li, Y., Morris, J. A., Overly, C. C., Parker, P. D., Parry, S. E., Reding, M., Royall, J. J., Schulkin, J., Sequeira, P. A., Slaughterbeck, C. R., Smith, S. C., Sodt, A. J., Sunkin, S. M., Swanson, B. E., Vawter, M. P., Williams, D., Wohnoutka, P., Zielke, H. R., Geschwind, D. H., Hof, P. R., Smith, S. M., Koch, C., Grant, S. G. N., and Jones, A. R. (2012) An anatomically comprehensive atlas of the adult human brain transcriptome. *Nature*. **489**, 391–399

Figure Captions

Figure 1.

Ykt6 is highly expressed in the hippocampus in the mammalian brain. A) Top, Sagittal view of the Ykt6 expression by in-situ hybridization assay and microarray with two Ykt6 probes in adult human brains. Allen Human Brain Atlas, https://human.brain-map.org/microarray/search/show?search_type=user_selections&user_selection_mode=2. Bottom panel, quantification of Ykt6 and Microtubule-associated protein 2 (MAP2) from the indicated brain regions (154). N=6 humans; MAP2 serves as a metric for high expression. Error bars represent standard deviation. **B)** Ykt6 expression by fluorescence in-situ hybridization in a sagittal section from a mouse brain. Allen Mouse Brain Atlas, https://mouse.brain-map.org/experiment/show/71380453.

Figure 2.

Ykt6 colocalizes with Golgi Apparatus, ER and mobilizes to the synapses in an activity-dependent manner. A-D) Primary hippocampal pyramidal neurons were immunostained at DIV21 with GM130 (Golgi Apparatus) and Ykt6. **A)** Representative immunofluorescence images of Golgi apparatus (magenta) and Ykt6 (cyan). **B)** Linescan of fluorescence intensities of Golgi apparatus and Ykt6 from the soma (Box 1) in (A). **C)** Secondary dendrites from (A). Golgi apparatus shown in magenta, Ykt6 in cyan. **D)** Fluorescence intensity linescans of the secondary dendrites from Box 2 in (A). **E-H)** Hippocampal pyramidal neurons were immunostained with protein disulfide isomerase (PDI) (ER) and Ykt6. **E)** Representative immunofluorescence images of ER (magenta) and Ykt6 (cyan). **F)** Linescan of fluorescence intensities of ER and Ykt6 from the soma (Box 1) in (E). **G)** Secondary dendrites from (E). ER shown in magenta, Ykt6 in cyan. **H)** Fluorescence intensity linescans of the secondary dendrites from Box 2 in (E). Scale bar = 10μm. **I)** Primary hippocampal neurons were exposed to glycine for chemical long-term potentiation (cLTP) or extracellular solution (ECS) as basal condition at DIV21 and labelled with a postsynaptic marker, postsynaptic density 95 (PSD95) and Ykt6. Each data point represents aggregate average of all calculated shortest distances of each PSD95 puncta present in a selected ROI from a secondary dendrite to the closest Ykt6 puncta. N=2, 30-50 cells per biological replicate. Unpaired T-test. * $p \leq 0.05$. **J-K)** Adult rat brain tissue was exposed to glycine (cLTP) or ECS (basal) and then fractionated to cysotosolic and synaptic fractions and probed for Ykt6 and GluA1; GAPDH serves as a loading control for the homogenate and the cytosolic fractions, and PSD95 serves as a loading control for the synaptosomal fraction. Representative western blot (J) with quantification over respective loading controls (K). N=4.

Figure 3.

Ykt6 mobilizes GluA1 to the synaptic terminals in an activity-dependent manner. A) Representative western blot for Ykt6 expression from hippocampal neurons co-transduced at DIV5 with Sh Ctrl RNA, Sh Ykt6 RNA and GFP construct, or Sh Ykt6 RNA and human Ykt6 tagged with GFP, was assayed for Ykt6 expression at DIV21. Left lane, solid arrow: endogenous Ykt6. Right lanes, dashed arrow: exogenous Ykt6. β-tubulin was used as a loading control. **B-C)** Hippocampal pyramidal neurons were co-transduced with either Sh Control RNA or Sh Ykt6 RNA, and GFP or GFP-tagged human Ykt6 at DIV5 and exposed to extracellular solution (ECS) or glycine for chemical long-term potentiation (cLTP) at DIV21, then immunolabelled for external and internal GluA1. **B)** Representative immunofluorescence images of the secondary dendrites. Internal GluA1 in red, external GluA1 in green. Scale bar = 10μm. **C)** Ratios of external to internal GluA1 levels, normalized to the control (basal condition, co-transduced with Sh Ctrl RNA and GFP construct). One-way ANOVA with Welch's correction and Dunnett's multiple comparisons test. * $p \leq 0.05$, ** $p \leq 0.01$, *** $p \leq 0.001$, **** $p \leq 0.0001$. N=3, 8-10 cells per replicate.

Figure 4.

Ykt6 modulates both pre- and post-synaptic terminals of glutamatergic neurotransmission. Hippocampal pyramidal neurons were transduced with Sh Ctrl RNA or Sh Ykt6 RNA at DIV5, then patch-clamped in whole-cell configuration between DIV18-21 in the presence of tetrodotoxin (TTX), D-2-Amino-5-phosphonovalerate (D-APV), and picrotoxin (PTX) to isolate AMPA currents. A-B) Quantification of amplitude per neuron for Sh Ctrl RNA-transduced and Sh Ykt6 RNA-transduced neurons. **A)** Cumulative distribution of the amplitudes for all events per condition. **B)** Average amplitude per condition. **C-D)** Quantification of frequency of events for Sh Ctrl RNA-transduced and Sh Ykt6 RNA-transduced neurons. **C)** Cumulative distribution of time between each event for every event per condition. **D)** Average frequency of events for each condition. Sh Ykt6-transduced neurons' distribution is significantly different from Sh Ctrl-transduced neurons' ($p < 0.0001$, Kolmogorov-Smirnov test). **E)** Representative traces of Sh Ctrl RNA-transduced and Sh Ykt6 RNA-transduced neurons. N=3, 4-6 cells per biological replicate. **F)** Hippocampal neurons were co-transduced at DIV5 with Sh Ctrl RNA and GFP construct, Sh Ykt6 RNA and GFP construct, or Sh Ykt6 RNA and human Ykt6 tagged with GFP and assayed for ATP levels at DIV21. N=3. **G-K)** Hippocampal neurons were transduced with Sh Ctrl RNA or Sh Ykt6 RNA at DIV5, then fixed at DIV21 and processed for electron microscopy (EM). **G)** Representative EM images of dendritic spines in Sh Ctrl RNA-transduced and Sh Ykt6 RNA-transduced neurons. **H)** Synaptic vesicle count for readily releasable pool. Each point is count for 1 image. **I)** Synaptic vesicle count for recycling pool. **J)** Synaptic vesicle count for reserve pool. **K)** Average synaptic vesicle size observed near synaptic contact points in Sh Ctrl RNA-transduced and Sh Ykt6 RNA-transduced neurons. Unpaired T-test with Welch's correction, * $p \leq 0.05$, ** $p \leq 0.01$, **** $p \leq 0.0001$.

Figure 5.

Dendritic arborization is dependent on Ykt6. Hippocampal pyramidal neurons were transduced with either Sh Control RNA or Sh Ykt6 RNA at DIV5, transfected with PGK-mCherry construct on DIV 19, and immunostained with mCherry at DIV21 and analyzed using Sholl analysis. **A)** Representative skeletonized images of Sh Ctrl-transduced or Sh Ykt6-transduced hippocampal pyramidal neurons. **B)** Quantification of maximum number of intersections for Sh Ctrl-transduced or Sh Ykt6-transduced hippocampal pyramidal neurons. **C)** Correlation of number of branches of hippocampal pyramidal neurons from (B) to the distance from the soma. Unpaired T-test with Welch's correction. * $p \leq 0.05$. N = 20-30, 10-15 cells per biological replicate. Scale bar: 100μm.

Supplemental Figure 1.

Ykt6 colocalizes with Golgi Apparatus and ER. A-H) Primary hippocampal pyramidal neurons were transduced with either either Sh Control RNA or Sh Ykt6 RNA at DIV5, and immunostained at DIV21 with GM130 (Golgi Apparatus) and Ykt6. **A)** Representative immunofluorescence images of Golgi apparatus (magenta) and Ykt6 (cyan) for Sh Control-transduced primary hippocampal pyramidal neurons. **B)** Linescan of fluorescence intensities of Golgi apparatus and Ykt6 from the soma (Box 1) in (A). **C)** Secondary dendrites from (A). Golgi apparatus shown in magenta, Ykt6 in cyan. **D)** Fluorescence intensity linescans of the secondary dendrites from Box 2 in (A). **E)** Representative immunofluorescence images of Golgi apparatus (magenta) and Ykt6 (cyan) for Sh Ykt6-transduced primary hippocampal pyramidal neurons. **F)** Linescan of fluorescence intensities of Golgi apparatus and Ykt6 from the soma (Box 1) in (E). **G)** Secondary dendrites from (E). Golgi apparatus shown in magenta, Ykt6 in cyan. **H)** Fluorescence intensity linescans of the secondary dendrites from Box 2 in (E). **I-P)** Primary hippocampal pyramidal neurons were transduced with either either Sh Control RNA or Sh Ykt6 RNA at DIV5, and immunostained with protein disulfide isomerase (PDI) (ER) and Ykt6. **I)** Representative immunofluorescence images of ER (magenta) and Ykt6 (cyan) for Sh Control-transduced primary hippocampal pyramidal neurons. **J)** Linescan of fluorescence intensities of ER and Ykt6 from the soma (Box 1) in (I). **K)** Secondary dendrites from (I). ER shown in magenta, Ykt6 in cyan. **L)** Fluorescence intensity linescans of the secondary dendrites from Box 2 in (I). **M)** Representative immunofluorescence images of ER (magenta) and Ykt6 (cyan) for Sh Ykt6-transduced primary hippocampal pyramidal neurons. **N)** Linescan of fluorescence intensities of ER and Ykt6 from the soma (Box 1) in (M). **O)** Secondary dendrites from (M). Golgi apparatus shown in magenta, Ykt6 in cyan. **P)** Fluorescence intensity linescans of the secondary dendrites from Box 2 in (M).

Supplemental Figure 2.

Supplemental Figure 2. Ykt6 loss of expression can be rescued with exogenous expression of Ykt6. A) Representative western blot for Ykt6 expression from hippocampal neurons co-transduced at DIV5 with Sh Ctrl RNA or Sh Ykt6 RNA at MOI 1.0, and GFP construct, human Ykt6 tagged with GFP, phosphomimetic mutant of human Ykt6 tagged with GFP (Mutant A), or phosphoablative mutant of human Ykt6 tagged with GFP (Mutant D) at various MOIs were assayed for Ykt6 expression at DIV21. Dashed arrow: exogenous Ykt6. Solid arrow: Endogenous Ykt6. β-tubulin was used as a loading control (**B).**

A

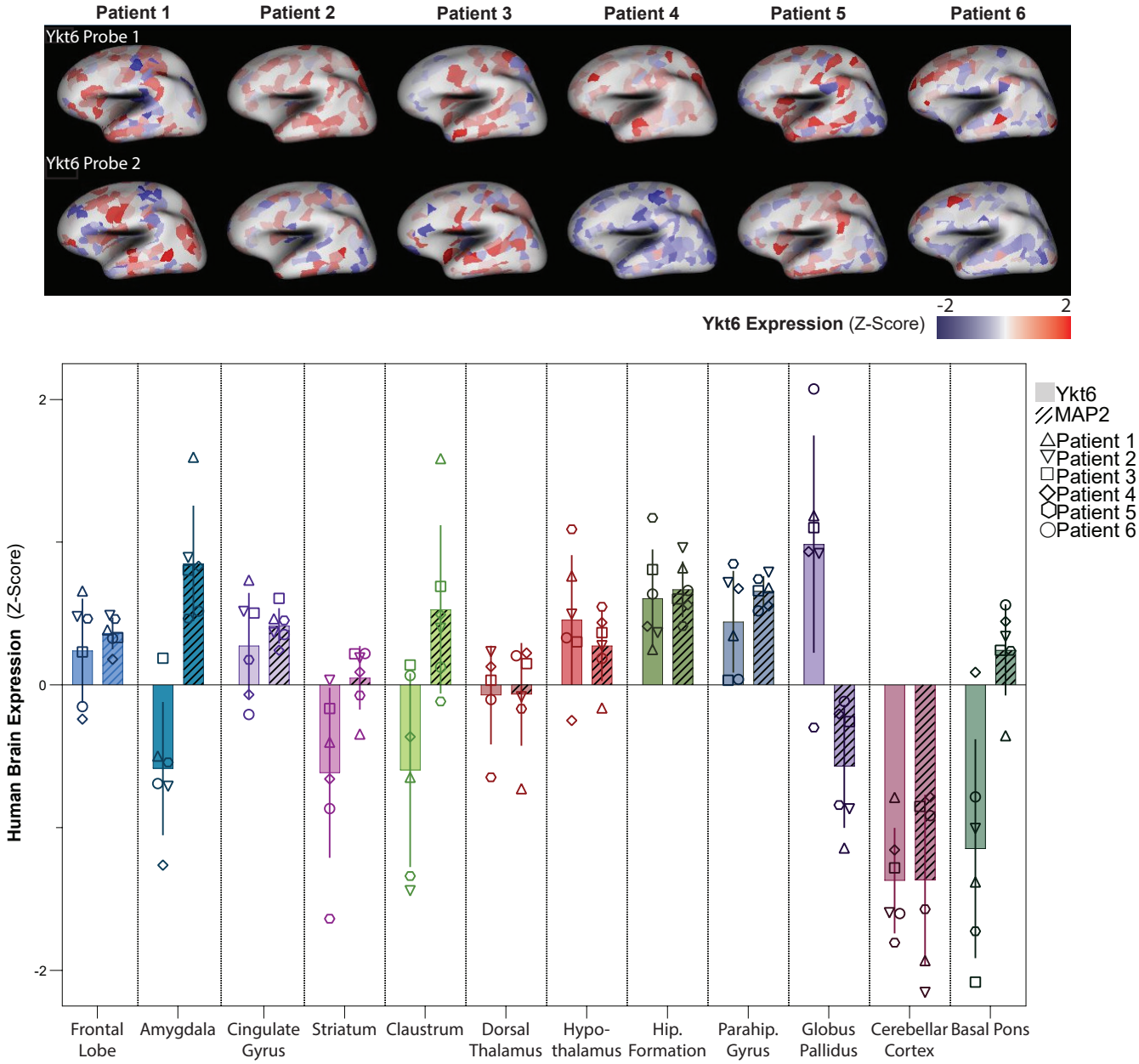
Patient 1
Patient 2
Patient 3
Patient 4
Patient 5
Patient 6
Ykt6 Probe 1
Ykt6 Probe 2
-2
2
Ykt6 Expression (Z-Score)
Human Brain Expression (Z-Score)
2
0
-2
Ykt6
MAP2
Patient 1
Patient 2
Patient 3
Patient 4
Patient 5
Patient 6
Frontal Lobe
Amygdala
Cingulate Gyrus
Striatum
Claustrum
Dorsal Thalamus
Hypo-thalamus
Hip. Formation
Parahip. Gyrus
Globus Pallidus
Cerebellar Cortex
Basal Pons

B

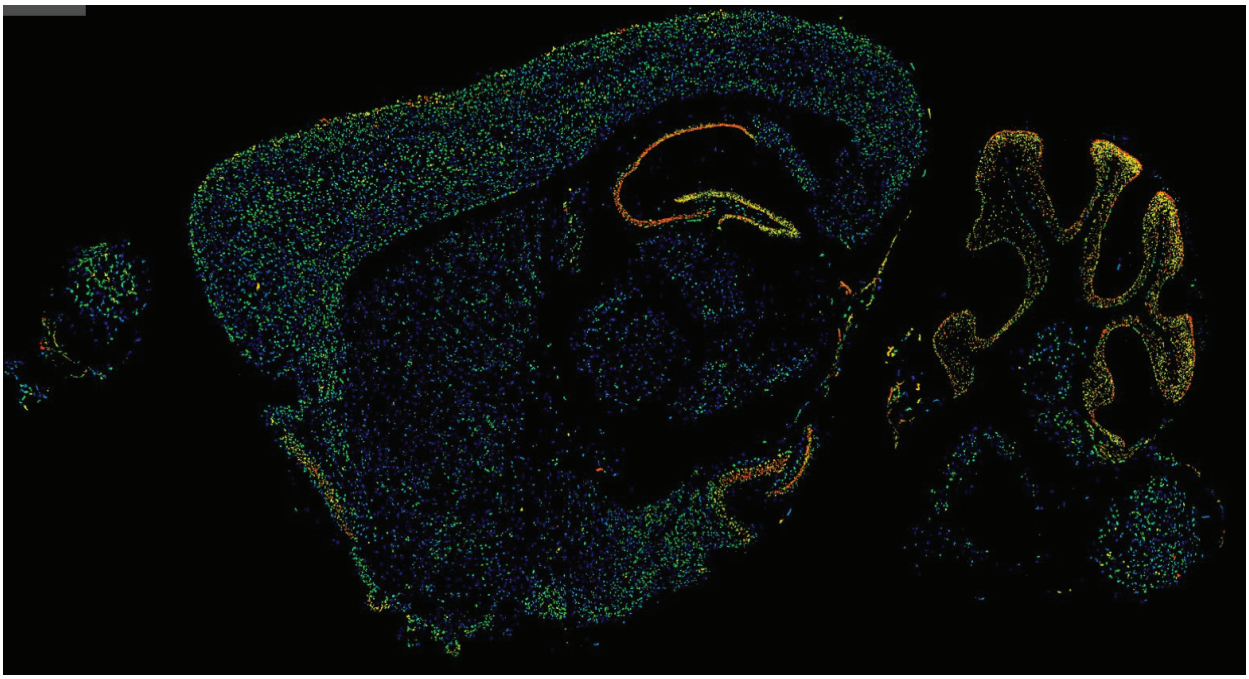

Figure 1.

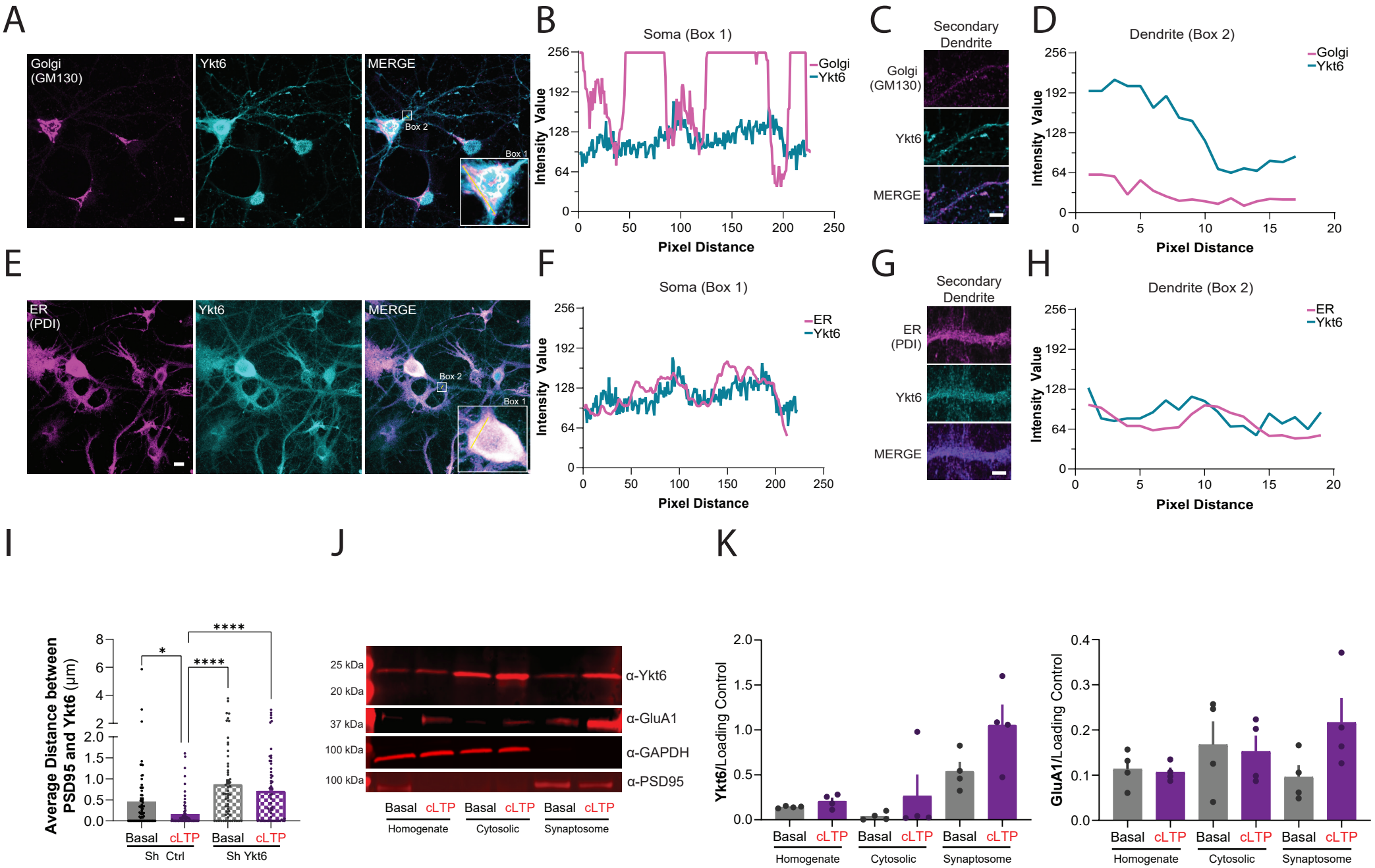
A
Golgi (GM130)
Ykt6
MERGE
Box 2
Box 1
B
Soma (Box 1)
Golgi
Ykt6
Intensity Value
Pixel Distance
C
Secondary Dendrite
Golgi (GM130)
Ykt6
MERGE
D
Dendrite (Box 2)
Golgi
Ykt6
Intensity Value
Pixel Distance
E
ER (PDI)
Ykt6
MERGE
Box 2
Box 1
F
Soma (Box 1)
ER
Ykt6
Intensity Value
Pixel Distance
G
Secondary Dendrite
ER (PDI)
Ykt6
MERGE
H
Dendrite (Box 2)
ER
Ykt6
Intensity Value
Pixel Distance
I
Average Distance between PSD95 and Ykt6 (µm)
Basal
cLTP
Sh Ctrl
Sh Ykt6
J
25 kDa
20 kDa
37 kDa
100 kDa
100 kDa
α-Ykt6
α-GluA1
α-GAPDH
α-PSD95
Basal
cLTP
Homogenate
Cytosolic
Synaptosome
K
Ykt6/Loading Control
GluA1/Loading Control
Basal
cLTP
Homogenate
Cytosolic
Synaptosome

Figure 2.

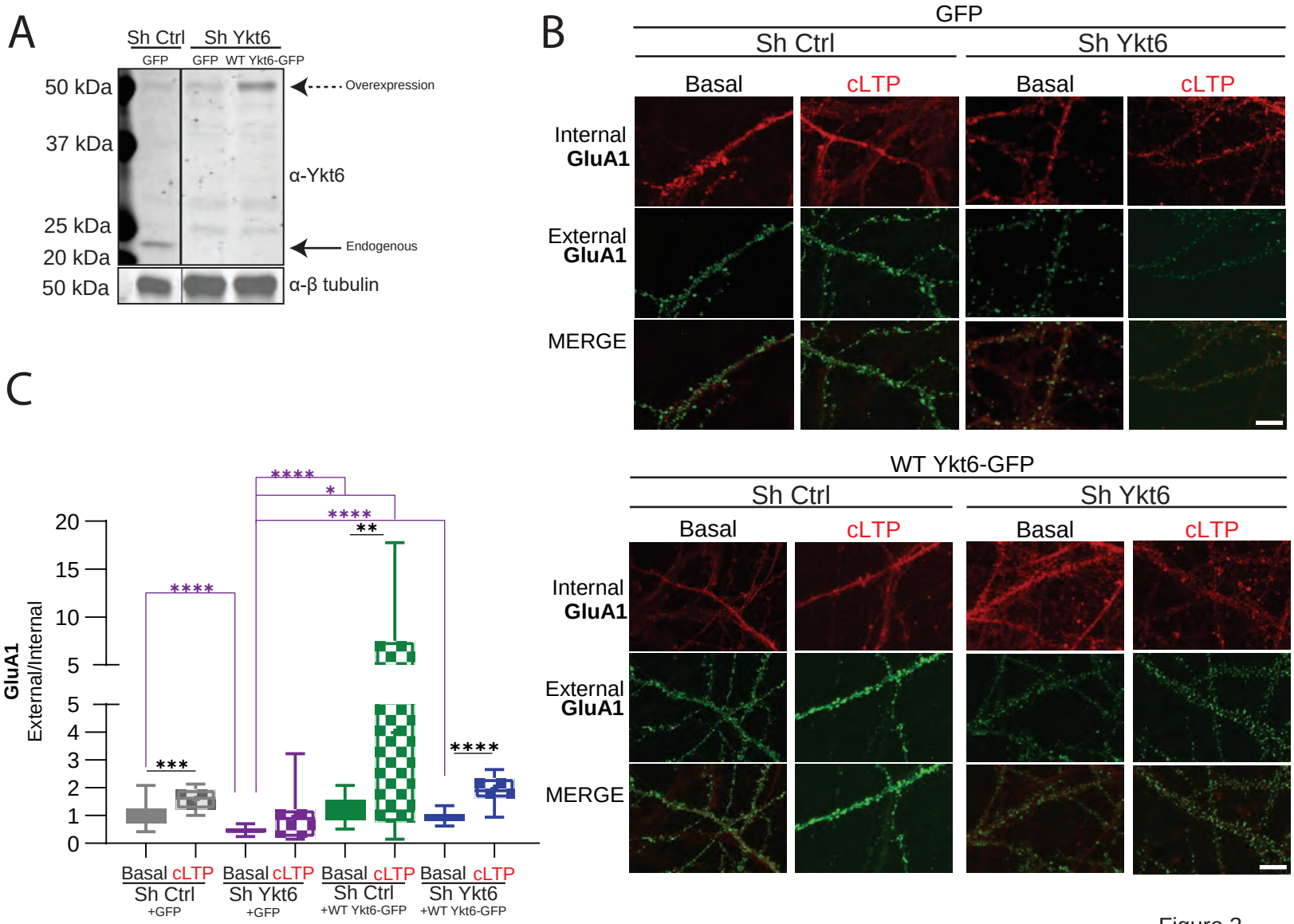
A
Sh Ctrl
Sh Ykt6
GFP
GFP
WT Ykt6-GFP
50 kDa
37 kDa
25 kDa
20 kDa
50 kDa
Overexpression
α-Ykt6
Endogenous
α-β tubulin
B
GFP
Sh Ctrl
Sh Ykt6
Basal
cLTP
Basal
cLTP
Internal GluA1
External GluA1
MERGE
WT Ykt6-GFP
Sh Ctrl
Sh Ykt6
Basal
cLTP
Basal
cLTP
Internal GluA1
External GluA1
MERGE
C
GluA1 External/Internal
20
15
10
5
5
4
3
2
1
0
****
*
****
**
****
***
****
Basal cLTP
Sh Ctrl +GFP
Basal cLTP
Sh Ykt6 +GFP
Basal cLTP
Sh Ctrl +WT Ykt6-GFP
Basal cLTP
Sh Ykt6 +WT Ykt6-GFP

Figure 3.

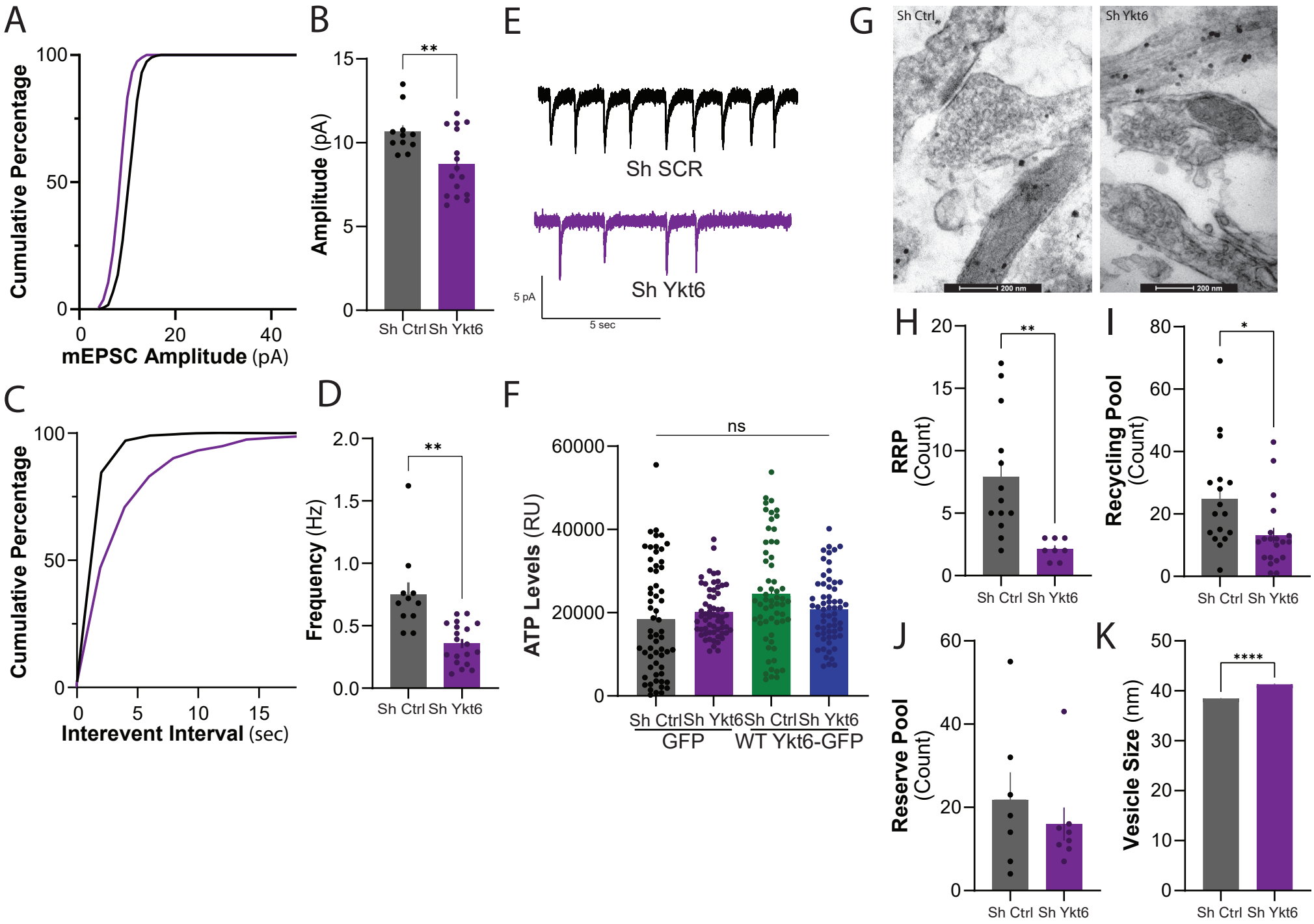
A
Cumulative Percentage
100
50
0
0
20
40
mEPSC Amplitude (pA)
B
Amplitude (pA)
15
10
5
0
**
Sh Ctrl
Sh Ykt6
E
Sh SCR
Sh Ykt6
5 pA
5 sec
G
Sh Ctrl
Sh Ykt6
200 nm
200 nm
C
Cumulative Percentage
100
50
0
0
5
10
15
Interevent Interval (sec)
D
Frequency (Hz)
2.0
1.5
1.0
0.5
0.0
**
Sh Ctrl
Sh Ykt6
F
ATP Levels (RU)
60000
40000
20000
0
ns
Sh Ctrl
Sh Ykt6
Sh Ctrl
Sh Ykt6
GFP
WT Ykt6-GFP
H
RRP (Count)
20
15
10
5
0
**
Sh Ctrl
Sh Ykt6
I
Recycling Pool (Count)
80
60
40
20
0
*
Sh Ctrl
Sh Ykt6
J
Reserve Pool (Count)
60
40
20
0
Sh Ctrl
Sh Ykt6
K
Vesicle Size (nm)
50
40
30
20
10
0
****
Sh Ctrl
Sh Ykt6

Figure 4.

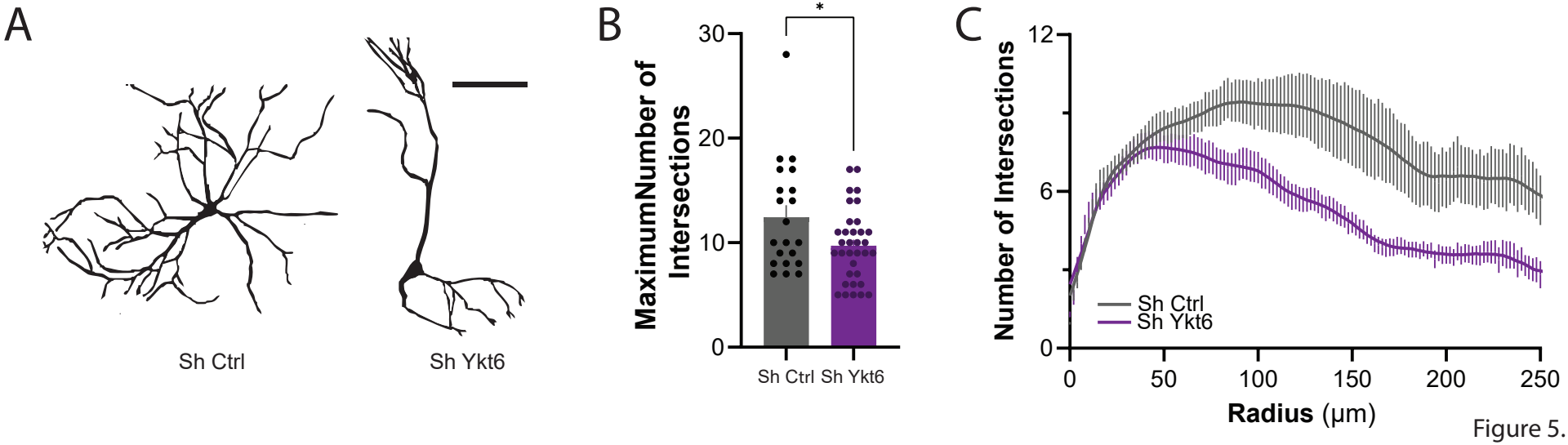
A
Sh Ctrl
Sh Ykt6
B
*
30
20
10
0
MaximumNumber of Intersections
Sh Ctrl
Sh Ykt6
C
12
6
0
Number of Intersections
Sh Ctrl
Sh Ykt6
0
50
100
150
200
250
Radius (μm)

Figure 5.